

---

1 Source attribution of near-surface ozone trends in the  
2 United States during 1995–2019

3  
4  
5  
6 Pengwei Li<sup>1</sup>, Yang Yang<sup>1\*</sup>, Hailong Wang<sup>2</sup>, Su Li<sup>1</sup>, Ke Li<sup>1</sup>, Pinya Wang<sup>1</sup>, Baojie  
7 Li<sup>1</sup>, Hong Liao<sup>1</sup>

8  
9  
10 <sup>1</sup>Jiangsu Key Laboratory of Atmospheric Environment Monitoring and  
11 Pollution Control, Jiangsu Collaborative Innovation Center of Atmospheric  
12 Environment and Equipment Technology, School of Environmental Science  
13 and Engineering, Nanjing University of Information Science and Technology,  
14 Nanjing, Jiangsu, China

15 <sup>2</sup>Atmospheric Sciences and Global Change Division, Pacific Northwest  
16 National Laboratory, Richland, Washington, USA

17  
18  
19  
20 \*Correspondence to yang.yang@nuist.edu.cn

---

21 **Abstract**

22 Emissions of ozone (O<sub>3</sub>) precursors in the United States have decreased  
23 in recent decades, and near-surface O<sub>3</sub> concentrations showed a significant  
24 decrease in summer but an increase in winter. In this study, an O<sub>3</sub> source  
25 tagging technique is utilized in a chemistry-climate model to investigate the  
26 source contributions to O<sub>3</sub> ~~concentrations~~mixing ratios in the U.S. from various  
27 emitting sectors and regions of nitrogen oxides (NO<sub>x</sub>) and reactive carbon  
28 species during 1995–2019. We show that domestic emission reductions from  
29 energy and surface transportation are primarily responsible for the decrease in  
30 summertime O<sub>3</sub> during 1995–2019. However, in winter, the emission control  
31 also weakens the NO<sub>x</sub> titration process, resulting in considerable increases in  
32 O<sub>3</sub> levels from natural sources. Additionally, increases in aviation and shipping  
33 ~~activities~~emissions and transpacific transport of O<sub>3</sub> from Asia largely contribute  
34 to the winter O<sub>3</sub> increase. ~~Changes~~We also found that changes in large-scale  
35 circulation favoring O<sub>3</sub> transport from upper atmosphere and foreign transport  
36 from Asia also explain 15% of the ~~O<sub>3</sub>-increasing trend~~increase in the U.S. near-  
37 surface O<sub>3</sub> levels in winter.

---

## 38 1. Introduction

39 Ozone (O<sub>3</sub>) near the surface has a significant impact on air quality and  
40 public health (Haagen-Smit, 1952; Fleming et al., 2018). Since the increase in  
41 anthropogenic emissions of O<sub>3</sub> precursors from preindustrial times, O<sub>3</sub> has now  
42 become the third most important anthropogenic greenhouse gas in the  
43 troposphere (Myhre et al., 2013). Major sources of O<sub>3</sub> in the troposphere  
44 include the transport from the stratosphere and formation through  
45 photochemical reactions within the troposphere involving two chemically  
46 distinct groups of precursors: nitrogen oxides (NO<sub>x</sub>) and reactive carbon  
47 species, including carbon monoxide (CO), methane (CH<sub>4</sub>), and non-methane  
48 volatile organic compounds (NMVOCs) (Atkinson, 2000). O<sub>3</sub> precursors come  
49 from a variety of sectors, and its relatively long lifetime of about 22 days  
50 (Stevenson et al. 2006) favors the long-range transport of O<sub>3</sub>. Due to the  
51 nonlinearity of the O<sub>3</sub> production and its associated dependence on precursor  
52 emissions (Seinfeld and Pandis, [19972006](#)), attributing O<sub>3</sub> pollution to its  
53 sources is complicated.

54 Since the 1980s, O<sub>3</sub> precursor emissions have significantly reduced in the  
55 United States (Duncan et al., 2016; Xing et al., 2013; Zhang et al., 2016; Zhang  
56 et al., 2021). However, due to the nonlinear production chemistry of O<sub>3</sub>,  
57 complex seasonal meteorological influence, and long-range transport from  
58 foreign source regions, domestic emissions reductions do not imply a decrease  
59 in seasonal and annual O<sub>3</sub> concentrations. According to remote surface  
60 measurements (Cooper et al., 2020) and aircraft observations (Gaudel et al.,  
61 2020), the Sixth Assessment Report of the Intergovernmental Panel on Climate  
62 Change (Szopa et al., 2021) showed a decreasing trend in annual mean O<sub>3</sub>  
63 concentrations in the western U.S. but an increasing trend in the eastern U.S.  
64 since the mid-1990s. On the seasonal timescale, surface observations and  
65 modeling results showed that O<sub>3</sub> concentrations over the U.S. had decreased

---

66 in summer due to the reductions in domestic anthropogenic emissions and  
67 increased in winter related to the weakened NO<sub>x</sub> titration since the late 1980s  
68 (Cooper et al., 2012; Lin et al., 2017). It also shows that the increased  
69 background O<sub>3</sub>, especially due to an increased transport from Asia, can partly  
70 offset the benefit of domestic emissions control over the western U.S. in  
71 summer.

72 Source apportionment is a useful method for quantifying contributions to  
73 air pollutants from specific source regions and/or sectors, which is beneficial to  
74 emission control strategies (Yang et al., 2018). One method of obtaining an O<sub>3</sub>  
75 source-receptor relationship is to zero out or perturb emissions from a given  
76 source region or sector in sensitivity simulations along with a baseline  
77 simulation, which gives information about the response of O<sub>3</sub> to changes in  
78 precursor emissions (e.g., Fiore et al., 2009; Hoor et al., 2009). However,  
79 emission perturbation method requires many additional model simulations  
80 when being used to estimate the ~~contributions~~impacts of changes in multiple  
81 sources (Koo et al., 2009; Wang et al., 2014) ~~and the~~. The perturbation method  
82 may invalidate the assumption of a linear relationship between the magnitude  
83 of the emission perturbation and the magnitude of the O<sub>3</sub> change considering  
84 the nonlinearity in O<sub>3</sub> chemistry, especially if large perturbations (e.g. zeroing  
85 out regional or sector-wide emissions) are used. The tagging approach  
86 produces information about the contribution of precursor emissions to the total  
87 amount of O<sub>3</sub> (Butler et al., 2020). The perturbation and tagging methods are  
88 two different methods answering different scientific questions, with the first for  
89 the impacts and the last for the contributions (Grewe et al. 2010, Emmons et al.  
90 2012, Clappier et al. 2017 and Thunis et al., 2019). Both of these two methods  
91 can be used for specific purpose to provide a comprehensive understanding of  
92 source-receptor relationships between precursor emissions and O<sub>3</sub>  
93 concentrations.

---

94 The source tagging method has been widely adopted in regional air quality  
95 models to examine the O<sub>3</sub> attribution in the U.S., China, and/or Europe (~~Collet~~  
96 ~~et al., 2022~~; Gao et al., 2016; [Collet et al., 2018](#); Lupaşcu and Butler, 2019). In  
97 some regional models, O<sub>3</sub> apportionment is based on the ratio of chemical  
98 indicators to determine the regime of O<sub>3</sub> generation (e.g., VOC-limited or NO<sub>x</sub>-  
99 limited regimes) and then attribute the generation of O<sub>3</sub> to the tag carried by a  
100 certain precursor (VOCs or NO<sub>x</sub>), which however cannot simultaneously  
101 attribute O<sub>3</sub> production to NO<sub>x</sub> and VOCs, respectively (Dunker et al., 2002;  
102 Kwok et al., 2015), while some models do not use the chemical indicators  
103 (Lupaşcu and Butler, 2019; Mertens et al., 2020). In addition, due to the  
104 limitation in domain size of regional air quality models, they are difficult to  
105 account for contributions of intercontinental transport from several sources  
106 outside the model domain. Recently, O<sub>3</sub> tagging techniques have been  
107 implemented in the global models (e.g., ~~Bates and Jacob, 2020~~; ~~Han et al.,~~  
108 ~~2018~~; Sudo and Akimoto, et al., 2007; Zhang et al., 2008; [Emmons et al., 2012](#);  
109 [Grewe et al. 2017](#); [Butler et al., 2018](#); [Han et al., 2018](#); [Bates and Jacob, 2020](#)).  
110 However, in many global models, O<sub>3</sub> is tagged by the production regions rather  
111 than the precursor emission regions, so that O<sub>3</sub> can only be attributed to the  
112 area where O<sub>3</sub> is generated, rather than the source of precursor emissions.

113 Here, based on a state-of-the-art tagging system implementation in a  
114 global chemistry–climate model, the trends of near-surface O<sub>3</sub>  
115 ~~concentrations~~[mixing ratios](#) in the U.S. during 1995–2019 and the source  
116 attributions of the O<sub>3</sub> variations to various emission sectors and regions of NO<sub>x</sub>  
117 and reactive carbon species are investigated in this study. Mechanisms of  
118 explaining the O<sub>3</sub> trends that involve changes in anthropogenic emissions and  
119 large-scale circulations are also explored.

## 120 **2. Methods**

### 121 **2.1 Model Description**

---

122 Tropospheric O<sub>3</sub> ~~concentrations~~mixing ratios are simulated using the  
123 Community Atmosphere Model version 4 with Chemistry (CAM4-chem)  
124 (Lamarque et al., 2012; Tilmes et al., 2015), which is the atmospheric chemistry  
125 component of the Community Earth System Model (CESM), at a horizontal  
126 resolution of 1.9° latitude by 2.5° longitude with 26 vertical levels extending to  
127 40 km above the surface. The height of bottom layer ~~near the surface~~ is about  
128 120 m and there are about 4 layers under 2 km. The model configuration uses  
129 a comprehensive tropospheric chemistry mechanism based on the Model for  
130 Ozone and Related chemical Tracers version 4 (MOZART-4) (Emmons et al.,  
131 2010, 2012). Model configurations simulate wet deposition of gas species using  
132 the Neu and Prather (2012) scheme. Dry deposition is represented following  
133 the resistance approach originally described in Wesely (1989). Stratosphere-  
134 troposphere exchange of O<sub>3</sub> is treated by setting O<sub>3</sub> to stratospheric values as  
135 their climatological means over 1996–2005 at the tropopause (Lamarque et al.,  
136 2012), which is affected by atmospheric circulation and experiences the same  
137 loss rates as O<sub>3</sub> in the troposphere (Tilmes et al., 2016). Sea surface  
138 temperatures and sea ice concentrations in our simulations are prescribed at  
139 present-day climatological conditions. The zonal and meridional wind fields are  
140 nudged towards the MERRA-2 (Modern Era Retrospective-Analysis for  
141 Research and Applications Version 2) reanalysis (Gelaro et al., 2017) at a 6-  
142 hourly relaxation timescale in this study to better constrain large-scale  
143 circulations by observations. The CAM4-chem performance in simulating  
144 tropospheric O<sub>3</sub> and precursors has been fully evaluated in Tilmes et al. (2015).

## 145 **2.2 Ozone Source Tagging Technique**

146 The novel O<sub>3</sub> source tagging technique implemented in the model was  
147 developed by Butler et al. (2018), which can provide a separate source  
148 apportionment of tropospheric O<sub>3</sub> to the two distinct groups of precursor  
149 emissions, i.e., NO<sub>x</sub> and reactive carbon (CO, CH<sub>4</sub> and NMVOCs). The portion

---

150 of tropospheric O<sub>3</sub> that is attributable to the stratosphere-troposphere exchange  
151 can also be quantified using this unique tagging technique. The source  
152 attribution of O<sub>3</sub> requires two separate model runs with the tagging applied to  
153 NO<sub>x</sub> and reactive carbon species, respectively. Details of the O<sub>3</sub> tagging  
154 technique are described in Butler et al. (2018).

155 In this study, near-surface O<sub>3</sub> is attributed to emission sectors and regions.  
156 Emissions from individual sectors, including agriculture (AGR), energy (ENE),  
157 industry (IND), residential, commercial and other (RCO), surface transportation  
158 (TRA), waste management (WST), international shipping (SHP) and biomass  
159 burning (BMB) emissions, as well as chemical production in the stratosphere  
160 (STR) and extra chemical production (XTR, a small amount of O<sub>3</sub> produced due  
161 to the self-reaction of OH radicals and the reactions of HO<sub>2</sub> with certain organic  
162 peroxy radicals) are tagged for both NO<sub>x</sub> and reactive carbon species. Aircraft  
163 (AIR), soil (SOIL) and lightning (LGT) sources are separately tagged for NO<sub>x</sub>  
164 emissions, while solvents (SLV) and biogenic (BIO) sources are separately  
165 tagged for NMVOCs emissions.

166 For the regional source attribution, we separately tag anthropogenic  
167 sources from Africa (AFR), Central America (CAM), Europe (EUR), Middle East  
168 (MDE), North America (NAM), East Asia (EAS), South Asia (SAS), Southeast  
169 Asia (SEA) and rest of the world (ROW) (see Fig. 1 for the region map) and  
170 natural sources (BMB, SOIL, LGT, BIO, STR and XTR). Additional tags for  
171 methane (CH<sub>4</sub>) and carbon monoxide (CO) are applied in both of the reactive  
172 carbon tagging simulations that are used to attribute O<sub>3</sub> to emission sectors and  
173 regions. We ~~does do~~ not tag CH<sub>4</sub> by individual sources and ~~its contribution is~~  
174 the contributions of CH<sub>4</sub> from various sources are lumped, ~~–~~ in this study. It is  
175 because CH<sub>4</sub> ~~is often considered separately from NMVOCs. It~~ has a relative  
176 long lifetime in the troposphere and it is well mixed in the troposphere due to its  
177 exceptionally low reactivity, which can contribute to O<sub>3</sub> formation at any location

---

178 in the troposphere where photochemical conditions are favorable (Fiore et al.,  
179 2008). CO also has a longer lifetime and lower reactivity than most NMVOCs;  
180 ~~separately tagging of CO is more conducive to distinguish its contribution to O<sub>3</sub>~~  
181 ~~from other NMVOCs. Therefore, the~~ The lumped ~~total~~ CO is ~~separately~~ tagged  
182 in the ~~sector attribution~~ simulations for emission sectors, but ~~the CO is~~ not  
183 specifically tagged in the ~~regional attribution~~ simulations for emission regions  
184 due to the computational limit.

### 185 **2.3 Emissions and Observation**

186 The global anthropogenic emissions, including NO<sub>x</sub>, CO, NMVOCs, SO<sub>2</sub>,  
187 and NH<sub>3</sub>, over 1990–2019 are from the Community Emissions Data System  
188 (CEDS) version 20210205 (Hoesly et al., 2018) (See Table S1 and Figs. S1–  
189 S3). Biomass burning emissions are obtained from the CMIP6 (Coupled Model  
190 Intercomparison Project Phase 6) over 1990–2014 (van Marle et al., 2017) and  
191 the emissions for the following five years (2015–2019) are interpolated from the  
192 SSP2-4.5 forcing scenario (O'Neill et al., 2016). NO<sub>x</sub> emitted from soils and  
193 biogenic NMVOCs from vegetation are prescribed as in Tilmes et al. (2015) and  
194 are kept at the present-day (2000) climatological levels during simulations.  
195 Lightning emissions of NO<sub>x</sub> are estimated online using ~~online~~the  
196 parameterization based on simulated cloud top heights from Price et al. (1997),  
197 which is scaled to provide a global annual emission of 3–5 Tg N yr<sup>-1</sup> ~~as~~  
198 ~~(Lamarque et. al. (, 2012)~~. CH<sub>4</sub> ~~mixing ratio~~ is fixed at a global average level of  
199 ~~4750~~1760 parts per billion (ppb, volume ratio in this study) during simulations.

200 Many studies have reported that the previous CEDS version 20160726  
201 (hereafter CEDS<sub>2016</sub>) has large biases in the regional emission estimates (e.g.,  
202 Cheng et al., 2021; Fan et al., 2018). In this study, the CEDS version 20210205  
203 is used (hereafter CEDS<sub>2021</sub>), which builds on the extension of the CEDS  
204 system described in McDuffie et al. (2020) and extends the anthropogenic  
205 emissions to year 2019. It updates country-level emission inventories for North



---

206 America, Europe and China and has considered the significant emission  
207 reductions in China since the clean air actions in recent years. The global total  
208 NO<sub>x</sub> emission from CEDS<sub>2021</sub> is lower than that of CEDS<sub>2016</sub> after 2006 and it  
209 shows a fast decline since then. In 2014, the global total anthropogenic  
210 emission of NO<sub>x</sub> in CEDS<sub>2021</sub> is about 10% lower than the CEDS<sub>2016</sub> estimate.  
211 This difference is mainly reflected in the NO<sub>x</sub> emissions in China and India.  
212 CEDS<sub>2021</sub> has a lower estimate of the global NMVOCs emission than CEDS<sub>2016</sub>  
213 by more than 10% during the recent decades, attributed to lower emissions  
214 from Africa, Central and South America, the Middle East and India. The using  
215 of the CEDS<sub>2021</sub> emission inventory in this study could reduce the contributions  
216 of NO<sub>x</sub> emissions from East Asia and South Asia to the U.S. O<sub>3</sub> mixing ratios  
217 and trends, as compared to CEDS<sub>2016</sub>. However, recent study reported a  
218 difference in aviation emission distribution of NO<sub>x</sub> between CMIP5 and CMIP6  
219 related to an error in data pre-processing in CEDS, leading to a northward shift  
220 of O<sub>3</sub> burden in CMIP6 (Thor et al., 2023). Therefore, the contribution of the  
221 aircraft emissions of NO<sub>x</sub> to the O<sub>3</sub> mixing ratios could be overestimated at high  
222 latitude regions.

223 Surface O<sub>3</sub> measurements in the U.S. are obtained from the U.S.  
224 Environmental Protection Agency (EPA). Linear trends of surface O<sub>3</sub> are  
225 calculated separately for boreal summer (June-July-August, JJA) and winter  
226 (December-January-February, DJF). Seasonal mean for any site that has less  
227 than 50% data availability in any month of a season is ~~not calculated.~~discarded  
228 following Lin et al. (2017). O<sub>3</sub> trends ~~at sites is shown~~calculated only when the  
229 seasonal data availability is greater than 85% during the analyzed period (more  
230 than 22 years). Trends in this study are calculated based on the linear least-  
231 squares regressions and the statistical significance is identified through the F  
232 test with the 95% confidence level.

## 233 **2.4 Experimental Design**

---

234 In this study, four groups of experiments are conducted, each group  
235 includes both NO<sub>x</sub> tagging simulation and reactive carbon tagging simulation.  
236 Two BASE experiment groups include simulations with emission sectors and  
237 regions, respectively, tagged for the two chemical distinct precursors. The  
238 BASE experiments are performed with time-varying anthropogenic emissions  
239 and winds nudged to MERRA-2 reanalysis. The other two groups of sensitivity  
240 experiments (MET) are the same as BASE experiments, except that the  
241 anthropogenic emissions are held at year 2019 level during simulations. All  
242 experiments are performed over 1990–2019, with the first 5 years treated as  
243 model spin-up and the last 25 years used for analysis. The BASE experiments  
244 are analyzed to quantify the source attributions of O<sub>3</sub> in the U.S., unless stated  
245 otherwise. We note that although the wind fields are nudged at a 6-hourly  
246 relaxation timescale, the atmospheric dynamics could also be slightly different  
247 between simulations, leading to the slight changes in the contributions from the  
248 same tags between simulations.

## 249 2.5 Model Evaluation

250 Figure S42 compares the simulated near-surface O<sub>3</sub> concentrationsmixing  
251 ratios with those from observations in 1995 and 2019, respectively. In general,  
252 the model overestimates O<sub>3</sub> concentrationsmixing ratios in the U.S. in both  
253 summer and winter by 10–40%. It can capture the seasonal pattern of O<sub>3</sub>  
254 seasonality—that high concentrationsmixing ratios in summer and low  
255 concentrationsmixing ratios in winter. The spatial distributions can also be  
256 roughly captured by the model, with statistically significant correlation  
257 coefficients between simulations and observations in the range of 0.21–0.45.  
258 From 1995 to 2019, the O<sub>3</sub> concentrationsmixing ratios in the U.S. decreased  
259 in summer and increased in winter presented in observations. The model can  
260 produce the sign of the changes, but has large biases in magnitudes, which will  
261 be discussed in the following section.

---

262

## 263 **3 Results**

### 264 **3.1 Ground-level ozone trends in the U.S.**

265 Emissions of O<sub>3</sub> precursors have substantially reduced since 1995 in both  
266 the western U.S. (WUS, 100–125°W, 30–45°N) and eastern U.S. (EUS, 70–  
267 100°W, 30–45°N), primarily owing to the reductions in anthropogenic  
268 emissions (Figs. S1–S3). However, the simulated annual near-surface O<sub>3</sub>  
269 ~~concentrations~~mixing ratios present opposite trends between WUS and EUS,  
270 with increases in EUS but weak decreases in WUS, which also exist in  
271 observations (Fig. ~~2a3a~~).

272 ~~Looking at different seasons, we found the~~The simulated contrasting  
273 trends in annual mean O<sub>3</sub> ~~concentrations~~mixing ratios between the WUS and  
274 EUS are dominated by the strong decreases in O<sub>3</sub> ~~concentrations~~mixing ratios  
275 in summer across the U.S. (Fig. ~~3b~~) and increased O<sub>3</sub> levels in winter over the  
276 central-eastern U.S. during 1995–2019. (~~Fig. 3c~~). The opposite trends between  
277 summer and winter have also been noted in many previous studies (e.g.,  
278 Copper et al., 2012; Lin et al., 2017, Jaffe et al., 2018). The model reproduces  
279 the observed O<sub>3</sub> trend over EUS in summer and roughly captures the O<sub>3</sub> trend  
280 over WUS in winter (Table ~~S41~~). The decreasing trend over WUS in summer  
281 and increasing trend over EUS in winter, however, are largely overestimated in  
282 the model, partly attributed to the coarse model resolution. The model also  
283 tends to overestimate the weakening of NO<sub>x</sub> titration in winter, leading to the  
284 biases. For spring and autumn, they are the transition between summer and  
285 winter, having the similar spatial pattern of O<sub>3</sub> trends as annual average, and  
286 will not be concerned in this study.

### 287 **3.2 Source attribution of ozone trends to emission sectors**

288 During 1995–2019, summer and winter NO<sub>x</sub> emissions from energy and  
289 surface transport sectors have significantly decreased in both WUS and EUS,

---

290 followed by industry and residential sectors, while those from aircraft have  
291 increased slightly (Fig. 34). Emissions of NMVOCs from surface transportation,  
292 solvents, industry, residential and waste sectors have decreased across the  
293 U.S., while those from energy and agriculture have increased. CO emissions  
294 have also significantly decreased over this time period.

295 ~~The O<sub>3</sub> trends in the U.S. attributed to different emission source sectors~~  
296 ~~are shown in Fig. 5.~~ The time series of the source sector contributions to O<sub>3</sub>  
297 mixing ratios from NO<sub>x</sub> and reactive carbon emissions are shown in Figs. 4,  
298 respectively Fig. 5 and the O<sub>3</sub> trends in the U.S. attributed to different emission  
299 source sectors are shown in Fig. 6. In summer, the O<sub>3</sub> attributed to NO<sub>x</sub>  
300 emissions from energy and surface transportation ~~NO<sub>x</sub> emissions~~ decreased at  
301 the rate of  $2.0 \pm 0.172$  and  $1.6 \pm 0.172$  ppb/decade in WUS and  $3.2 \pm 0.152$  and  
302  $1.7 \pm 0.212$  ppb/decade in EUS, respectively (Figs. 5a6a and 5e6c). On the  
303 contrary, the O<sub>3</sub> contributed by aircraft NO<sub>x</sub> emissions increased by  $0.4 \pm 0.030$   
304 ppb/decade in both WUS and EUS. Along with the reductions in anthropogenic  
305 emissions, natural emissions are becoming increasingly important as sources  
306 for O<sub>3</sub> formation near the surface. Although NO<sub>x</sub> emissions from soil are held at  
307 the present-day climatological levels, they account for  $0.7 \pm 0.081$  and  $1.7 \pm 0.401$   
308 ppb/decade increase in WUS and EUS, respectively, during 1995–2019, related  
309 to the changing O<sub>3</sub> production efficiency under the more NO<sub>x</sub>-sensitive  
310 condition. Note that, during 1995–2019, the molar ratio (mol N /mol C) of  
311 emitted NO<sub>x</sub> to NMVOCs reduced from 0.11 to 0.07 in ~~the~~ WUS and from 0.14  
312 to 0.07 in ~~the~~ EUS, confirming the enhanced NO<sub>x</sub>-sensitive condition during the  
313 analyzed time period. In recent decades, global emissions from international  
314 shipping have increased rapidly (Eyring, et al., 2005; Müller-Casseres et al.,  
315 2021), but have declined near the coast of the United States. Due to a strong  
316 chemical sink associated with photolysis of O<sub>3</sub> with subsequent production of  
317 hydroxyl radical (OH) from water vapor in summer (Johnson et al., 1999), the

---

318 effect of increased international shipping emissions ~~of~~over the ~~far-shore~~remote  
319 ocean regions on the continental ~~United States~~U.S. was blunted. But the  
320 increase in shipping emissions inland tends to increase O<sub>3</sub>  
321 ~~concentrations~~mixing ratios in eastern U.S. (Fig. ~~S5~~S4).

322 In summer, biogenic sources dominate the emissions of NMVOCs in the  
323 U.S. (Fig. S3). As the O<sub>3</sub> decreases, mainly due to the reductions in domestic  
324 NO<sub>x</sub> emissions, the contributions from biogenic emissions of NMVOCs have a  
325 decreasing trend in the U.S. during 1995–2019 (Figs. ~~5b~~6b and ~~5d~~6d), even  
326 though biogenic emissions were fixed during simulations. This also applies to  
327 CH<sub>4</sub>, of which the ~~concentration~~mixing ratio was kept constant. This does not  
328 actually mean that CH<sub>4</sub> and biogenic NMVOCs themselves contributed to the  
329 overall O<sub>3</sub> trend through changing the precursor levels since they were kept  
330 constant during simulations; rather, mainly due to the reductions in NO<sub>x</sub>  
331 emissions, O<sub>3</sub> production efficiency by reactive carbon species decreases,  
332 leading to decreasing trends of O<sub>3</sub> contribution by CH<sub>4</sub> and biogenic NMVOCs.  
333 In conjunction with NO<sub>x</sub> emission reductions, decreases in NMVOCs emissions  
334 from surface transportation and industry sectors contribute negative O<sub>3</sub> trends  
335 of  $-0.3 \pm 0.0$  and  $-0.1 \pm 0.0$  ppb/decade, respectively, in both WUS and EUS, in  
336 summer (Figs 6b and 6d), which are offset by the increases in NMVOCs  
337 emissions from energy and agriculture sectors. Although the O<sub>3</sub> production  
338 efficiency of CO is relatively low, the contributions of CO to O<sub>3</sub>  
339 ~~concentrations~~mixing ratios largely decreased with trends of  $-0.6 \pm 0.1$  and  $-$   
340  $0.5 \pm 0.1$  ppb/decade in WUS and EUS, respectively, due to the massive  
341 reduction in anthropogenic emissions of CO (Fig. S1).

342 In winter, through the weakened NO<sub>x</sub> titration process (Gao et al., 2013;  
343 Simon et al., 2015), the NO<sub>x</sub> emission control causes an increase in O<sub>3</sub> levels  
344 during 1995–2019, especially the contribution from surface transportation  
345 ( $0.4 \pm 0.0$  ppb/decade in WUS and  $0.8 \pm 0.1$  ppb/decade in EUS) (Figs. ~~5e~~6e and

---

346 ~~5g6g~~). Although aircraft NO<sub>x</sub> emissions slightly increased, ~~but~~ O<sub>3</sub> attributed to  
347 aircraft NO<sub>x</sub> emissions shows positive trends as large as 0.4±0.0 and 0.6±0.0  
348 ppb/decade in WUS and EUS, respectively. It is because aircraft emissions are  
349 injected directly into the upper troposphere and lower stratosphere in a low  
350 ambient NO<sub>x</sub> condition and have a much higher O<sub>3</sub> enhancement efficiency  
351 than surface emissions (Hodnebrog et al., 2011). It can be confirmed that the  
352 NO<sub>x</sub> from aircraft contributes to the increase in O<sub>3</sub> ~~concentrations~~mixing ratios  
353 at 250 hPa in high latitude regions of the Northern Hemisphere during 1995–  
354 2019 (Fig. ~~S6S5~~). The decrease in near-shore shipping emissions weakened  
355 the NO<sub>x</sub> titration, together with the weakened O<sub>3</sub> chemical sink from water vapor  
356 in winter, leading to large increasing trends of O<sub>3</sub> by 0.8±0.1 and 1.0±0.1  
357 ppb/decade, respectively, in the WUS and EUS during 1995–2019. Although  
358 most natural emissions do not change during the simulations, the net O<sub>3</sub>  
359 chemical production is more sensitive to NO<sub>x</sub> under the emission control  
360 condition, resulting in the increasing O<sub>3</sub> trends contributed by the soil and  
361 lightning NO<sub>x</sub> emissions. Due to the weakened NO<sub>x</sub> titration in winter, the  
362 contribution of stratospheric intrusion increases at a rate of 0.6±0.1 and 1.0±0.1  
363 ppb/decade over WUS and EUS, respectively, when stratospheric contribution  
364 to the near-surface O<sub>3</sub> is relatively high (Butler et al., 2018). Along with the  
365 weakened NO<sub>x</sub> titration, contributions from reactive carbon emissions to the  
366 near-surface O<sub>3</sub> in the U.S. also increase for most species and sectors (Figs.  
367 ~~5f6f~~ and ~~5h6h~~).

### 368 **3.3 Source attribution of ozone trends to emission regions**

369 ~~The~~Time series of the source region contributions to near-surface O<sub>3</sub>  
370 mixing ratios are shown in Fig. 7 and the O<sub>3</sub> trends in the U.S. attributed to  
371 different emission source regions are presented in Fig. ~~7. Time series of the~~  
372 ~~source contributions are shown in Figs. 6g~~. In summer, domestic anthropogenic  
373 NO<sub>x</sub> emissions (excluding those from soil) within North America account for 49%

374 of the near-surface O<sub>3</sub> ~~concentration~~mixing ratio averaged over the U.S.  
375 (WUS+EUS) in 1995–2019. The domestic emission reduction is the dominant  
376 factor causing the decline in surface O<sub>3</sub> ~~concentrations~~mixing ratios, with  
377 contributions of  $-4.4 \pm 0.222$  and  $-5.7 \pm 0.3$  ppb/decade to the trends over WUS  
378 and EUS, respectively, during 1995–2019 (Figs. [7a8a](#) and [7e8c](#)). Reductions in  
379 the NMVOCs emissions from North American anthropogenic sources also  
380 decrease O<sub>3</sub> ~~concentrations~~mixing ratios (Figs. [7b8b](#) and [7d8d](#)), accompanying  
381 with the domestic NO<sub>x</sub> emission control. The increase in NO<sub>x</sub> emissions from  
382 Asia contributes  $0.7 \pm 0.1$  ppb/decade to the total O<sub>3</sub> increasing trend in WUS,  
383 partly offsetting the negative impact of domestic emission reductions, but has a  
384 weak impact in EUS, which is consistent with previous studies (Lin et al., 2017).

385 In winter, domestic anthropogenic NO<sub>x</sub> emissions only account for 19% of  
386 the surface O<sub>3</sub> ~~concentration~~mixing ratio in the U.S. over 1995–2019, while NO<sub>x</sub>  
387 sources from lightning, rest of the world (mainly from the international shipping),  
388 and Asia contribute 17%, 14%, and 11%, respectively, ~~and~~. O<sub>3</sub> from  
389 stratospheric intrusion contributes 21% of the near-surface O<sub>3</sub> in the U.S. ([Fig. 6](#))  
390 ~~in winter~~. During 1995–2019, the significant increase in wintertime surface  
391 O<sub>3</sub> ~~concentrations~~mixing ratios are not directly linked to the reductions in  
392 domestic anthropogenic emissions (Figs. [7e8e](#) and [7g8g](#)). However, the  
393 domestic emission control weakens the NO<sub>x</sub> titration, resulting in considerable  
394 increases in O<sub>3</sub> originating from the natural sources, including O<sub>3</sub> from  
395 stratospheric intrusion, lightning and soil emissions. The natural sources  
396 combined contribute to positive O<sub>3</sub> trends of  $1.2 \pm 0.2$  and  $2.4 \pm 0.3$  ppb/decade  
397 in WUS and EUS, respectively. If the O<sub>3</sub> increase is attributed to NMVOCs  
398 emissions, the combined natural source contribution is even larger ( $1.4 \pm 0.2$  [in](#)  
399 [WUS](#) and  $2.5 \pm 0.2$  ppb/decade [in EUS](#)) (Figs. [7f8f](#) and [7h8h](#)). O<sub>3</sub> produced by  
400 CH<sub>4</sub> increases at rates of  $1.3 \pm 0.1$  and  $2.1 \pm 0.1$  ppb/decade in WUS and EUS,  
401 respectively, due to the weakened NO<sub>x</sub> titration. Increases in aviation and



---

402 shipping emissions together explain the  $1.2\pm 0.1$  and  $1.5\pm 0.1$  ppb/decade of O<sub>3</sub>  
403 trends in WUS and EUS, respectively (Figs. 5e6e and 5g6g). Long-range  
404 transport of O<sub>3</sub> produced from Asian NO<sub>x</sub> emissions enhances the wintertime  
405 O<sub>3</sub> increasing trends by  $0.9\pm 0.1$  and  $1.2\pm 0.1$  ppb/decade in WUS and EUS,  
406 respectively, which are equally contributed by sources from East Asia, South  
407 Asia, and Southeast Asia (Figs. 7e8e and 7g8g).

### 408 **3.4. Impact of variations in large-scale circulations on ozone trends**

409 Many studies have reported that O<sub>3</sub> spatial distribution is strongly  
410 modulated by changes in large-scale circulations (e.g., Shen and Mickley, 2017;  
411 Yang et al., 2014, 2022). Based on our MET experiments with anthropogenic  
412 emissions kept unchanged, the changes in large-scale circulations show a  
413 weak influence on the U.S. O<sub>3</sub> trends in summer (Fig. 8a9a) but cause a  
414 significant O<sub>3</sub> rise in the central U.S. in winter (Fig. 8b9b). Averaged over the  
415 U.S., the near-surface O<sub>3</sub> ~~concentration~~ mixing ratio in winter increases at the  
416 rate of  $0.7\pm 0.3$  ppb/decade during 1995–2019 in MET experiments, ~~accounting~~  
417 ~~for 15% of the trend of  $4.7\pm 0.3$  ppb/decade in BASE experiments.~~ It suggests  
418 that the variation in large-scale circulations is responsible for 15% of the  
419 ~~increase in wintertime O<sub>3</sub> concentrations in the U.S. over 1995–2019. Variations~~  
420 ~~in the circulation facilitate O<sub>3</sub> transport from upper altitudes to the surface, as~~  
421 ~~well as foreign contributions from Asia, which is consistent with the finding in~~  
422 ~~Lin et al. (2015). The O<sub>3</sub> increasing trend in winter over the U.S. attributing to~~  
423 ~~stratospheric injection and Asian NO<sub>x</sub> emissions due to dynamics are both~~  
424  ~~$0.2\pm 0.1$  ppb/decade (Fig. 8e). Therefore, changes in anthropogenic emissions~~  
425 ~~are the main factor affecting O<sub>3</sub> trends.~~ increasing trend in wintertime O<sub>3</sub> mixing  
426 ratio by  $4.7\pm 0.3$  ppb/decade in the U.S. during 1995–2019 simulated in BASE  
427 experiment.

428 The changes in atmospheric circulation pattern support the above finding.  
429 Compared to 1995–1999, anomalous northerly winds locate over high latitudes



---

430 of North America in 2015–2019 (Fig. 8e9c), strengthening the prevailing  
431 northerly winds in winter. ~~The strengthened winds transport O<sub>3</sub> from remote~~  
432 ~~regions (e.g., Asia) to the central U.S. (Fig. 8g).~~ In addition, an anomalous  
433 subsidence ~~also~~ occurs over the central U.S. in 2015–2019, compared to 1995–  
434 1999 (Fig. 8d), ~~leading to an 9d).~~ The anomalous downwardsubsidence  
435 transport of O<sub>3</sub> from high altitudes and even stratosphere to the surface (Figs.  
436 8g and 8h). and the strengthened winds transport O<sub>3</sub> from remote regions (e.g.,  
437 O<sub>3</sub> produced by Asian NO<sub>x</sub> emission) to the central U.S., both contributing to  
438 0.2±0.1 ppb/decade of the O<sub>3</sub> increase over the U.S. (Fig. 10). The ~~horizontal~~  
439 ~~and vertical~~ finding is consistent with Lin et al. (2015) that variations in the  
440 circulation facilitate O<sub>3</sub> transport of O<sub>3</sub> together contribute from upper altitudes  
441 to the near-surface O<sub>3</sub> increases in winter during 1995–2019 associated with  
442 the changes in large-scale circulations, as well as foreign contributions from  
443 Asia. The anomalous atmospheric circulation is likely linked to the location of  
444 the midlatitude jet stream, which is influenced by ENSO cycle ~~(Lin et al., 2015).~~

445

#### 446 **4. Conclusions and discussions**

447 Using a global chemistry–climate model equipped with an O<sub>3</sub> source  
448 tagging technique, we examine the long-term trends and source apportionment  
449 of O<sub>3</sub> in the continental U.S. over 1995–2019 to various emission source  
450 sectors and regions in this study. This model can capture the O<sub>3</sub> decreasing  
451 trend over the EUS in summer and increasing trend over the WUS in winter  
452 during this time period, but largely overestimates the decreasing trend over  
453 WUS in summer and increasing trend over EUS in winter.

454 In summer, our simulation results show that the decline in surface O<sub>3</sub> is  
455 dominated by the rapid reductions in NO<sub>x</sub> emissions from energy and surface  
456 transportation sectors, contributing to O<sub>3</sub> decreases at a rate of –2.0 and –1.6  
457 ppb/decade in WUS and –3.2 and –1.7 ppb/decade in EUS, respectively. As

---

458 the anthropogenic NO<sub>x</sub> decreases, the more NO<sub>x</sub>-sensitive condition leads to a  
459 positive O<sub>3</sub> trend of 0.7 and 1.7 ppb/decade in WUS and EUS, respectively,  
460 contributed by the NO<sub>x</sub> emissions from soil. Due to the reductions in NO<sub>x</sub>  
461 emissions, the O<sub>3</sub> production efficiency by reactive carbon species also  
462 decreased, leading to the decreasing contributions to O<sub>3</sub> from reactive carbon  
463 species in summer during 1995–2019. Even though biogenic NMVOCs  
464 emissions and CH<sub>4</sub> mixing ratio were fixed during simulations, their  
465 contributions also decreased related to the weakened O<sub>3</sub> production efficiency  
466 by these precursors. Source region tagging suggests that the domestic  
467 emission reductions are primarily responsible for the decreasing trend in  
468 summertime near-surface O<sub>3</sub> ~~concentrations~~mixing ratios in the U.S. during  
469 1995–2019.

470 The mechanisms of wintertime O<sub>3</sub> increases over the U.S. are more  
471 ~~complex~~complicated. First, the domestic emission control weakens the NO<sub>x</sub>  
472 titration, resulting in considerable increases in O<sub>3</sub> originating from natural  
473 sources, including O<sub>3</sub> from stratospheric intrusion, lightning, soil and biogenic  
474 emissions. The natural sources combined contribute a positive O<sub>3</sub> trend of more  
475 than 1 and 2 ppb/decade in WUS and EUS, respectively. Second, increases in  
476 aviation and shipping emissions together explain the 1.2 and 1.5 ppb/decade  
477 of O<sub>3</sub> trends in WUS and EUS, respectively. Third, long-range transport of O<sub>3</sub>  
478 produced from Asian NO<sub>x</sub> emissions enhances the wintertime O<sub>3</sub> increasing  
479 trends by 0.9 and 1.2 ppb/decade in WUS and EUS, respectively. Fourth, the  
480 variation of horizontal and vertical transport O<sub>3</sub> associated with the changes in  
481 large-scale circulation contributes to the near-surface O<sub>3</sub> increases over the  
482 U.S. by 15% in winter during 1995–2019.

483 ~~The overestimate of O<sub>3</sub> trend in the EUS might be related to a potential~~  
484 ~~biased model representation of vertical mixing in winter.~~ Compared to  
485 observations, the decreasing trend of O<sub>3</sub> ~~concentrations~~mixing ratios over WUS

---

486 in summer and increasing trend over EUS in winter are overestimated in the  
487 CAM4-chem model. Because most O<sub>3</sub> monitors are located in urban areas and  
488 these areas generate strong O<sub>3</sub> during the day and have strong oxidation  
489 titration at night, the daily and grid averaged O<sub>3</sub> ~~concentrations~~mixing ratios  
490 output by the model could be inconsistent with the urban observations. The  
491 overestimate of O<sub>3</sub> trend in the EUS might be related to a potential biased model  
492 representation of vertical mixing in winter. ~~Besides,~~Large uncertainties existing  
493 in the emissions also result in the biases in the O<sub>3</sub> simulation. Lin et al. (2017)  
494 found that the contribution from increasing Asian emissions offset that from the  
495 U.S. emission reductions, resulting in a weak O<sub>3</sub> trend in WUS. In this study,  
496 the Asian NO<sub>x</sub> emissions only contribute to 0.6 ppb/decade of the total positive  
497 trend in WUS in summer, much lower than the 3.7 ppb/decade decrease  
498 attributable to the domestic emission reductions, suggesting that the Asian  
499 contribution to the O<sub>3</sub> trends in WUS is ~~likely~~possibly underestimated in this  
500 study. ~~The bias of~~We also found that the model did not capture the significant  
501 increase in summertime O<sub>3</sub> simulation levels in China ~~may also lead to a bias in~~  
502 ~~the wintertime O<sub>3</sub> trend over EUS~~in recent years, which could explain the low  
503 contribution from Asian sources. Additionally, international shipping can have a  
504 disproportionately high influence on tropospheric O<sub>3</sub> due to the dispersed  
505 nature of NO<sub>x</sub> emissions (Butler et al., 2020; Kasibhatla et al., 2000; von Glasow  
506 et al., 2003), together with the weakened NO<sub>x</sub> titration, resulting in the  
507 overestimation of O<sub>3</sub> trends. The fixed CH<sub>4</sub> mixing ratio during simulations also  
508 biased the modeled O<sub>3</sub> trends ~~in this study~~, which deserves further investigation  
509 with the varying CH<sub>4</sub> levels in future studies. The coarse model resolution also  
510 contributed to the biases. The overestimate of O<sub>3</sub> trend over EUS in winter,  
511 likely related to the bias in NO<sub>x</sub> titration, implies the overestimate of source  
512 contributions to the trends in magnitude.

513 Compared with Butler et al. (2018), the simulation in this study shares

---

514 similar source sector contributions to the zonal average of O<sub>3</sub>  
515 ~~concentrations~~mixing ratios at the surface and 400 hPa in 2010 (Figs. S7 and  
516 S8 in this study and Figs. 5 and 6 in Butler et al. (2018)). The contributions from  
517 the stratosphere and lightning NO<sub>x</sub> are relatively higher in this study than Butler  
518 et al. (2018). This may be related to the different anthropogenic emission  
519 inventories used, causing different O<sub>3</sub> production/loss efficiencies by natural  
520 precursors. When comparing the contributions from different source regions to  
521 surface O<sub>3</sub> ~~concentrations~~mixing ratios in North America, NO<sub>x</sub> emissions from  
522 East Asia, South Asia, North America, and Europe contributed 2.2, 1.1, 8.3, and  
523 0.7 ppb of the surface O<sub>3</sub> in North America, respectively (Fig. S9) in this study,  
524 which are also similar to those from Fig. 4 in Butler et al. (2020). Both studies  
525 show the contributions of anthropogenic NMVOCs to surface O<sub>3</sub>  
526 ~~concentrations~~mixing ratios in North America are less than 10 ppb.

527 ~~As the results of the study heavily depend on the emission inventory, here~~  
528 ~~the potential bias in emissions are also discussed. Compared with the previous~~  
529 ~~CEDS version used in this study (hereafter CEDS<sub>Hoesly</sub>), the updated CEDS~~  
530 ~~inventory (hereafter CEDS<sub>GBD-MAPS</sub>) (McDuffie et al., 2020) incorporates~~  
531 ~~updated activity data. For NO<sub>x</sub>, the global emission from CEDS<sub>GBD-MAPS</sub> is~~  
532 ~~smaller than that of CEDS<sub>Hoesly</sub> after 2006 and shows a fast decreasing trend.~~  
533 ~~By 2014, global emission of NO<sub>x</sub> is about 10 % lower than the CEDS<sub>Hoesly</sub>~~  
534 ~~estimate. These differences are mainly reflected in the industrial and residential~~  
535 ~~sectors in China, followed by the transportation sector in India and Africa. For~~  
536 ~~global emission of NMVOCs, which remains relatively unchanged between the~~  
537 ~~CEDS<sub>Hoesly</sub> and CEDS<sub>GBD-MAPS</sub> inventories (Fig. 6 in McDuffie et al. 2020). The~~  
538 ~~global NO<sub>x</sub> emission from EDGAR v4.3.2 inventory is less than CEDS<sub>Hoesly</sub>~~  
539 ~~(Grippa et al., 2018). This difference in NO<sub>x</sub> emissions may reduce O<sub>3</sub> trends in~~  
540 ~~U.S. from foreign contributions, especially from East Asia. Recent study also~~  
541 ~~reported a difference in NO<sub>x</sub> emission distribution between CMIP5 and CMIP6~~

---

542 ~~related to an error in data pre-processing in CEDS, leading to a northward shift~~  
543 ~~of O<sub>3</sub> burden in CMIP6 (Thor et al., 2023). The aviation emissions should be~~  
544 ~~corrected in future studies of O<sub>3</sub> simulations.~~

545

---

546 **Author contributions.** YY designed the research; PL and SL performed  
547 simulations; PL analyzed the data. All authors including HW, KL, PW, BL, and  
548 HL discussed the results and wrote the paper.

549

550 **Code and data availability.** The CESM is maintained by NCAR and is provided  
551 freely to the community. The ozone tagging code has been described by Butler  
552 et al. (2018). The MERRA-2 reanalysis data are from NASA GESDISC data  
553 (<https://goldsmr5.gesdisc.eosdis.nasa.gov/data/MERRA2/M2I6NVANA.5.12.4/>,  
554 last access: 1 August 2022). The surface O<sub>3</sub> measurements in U.S. are  
555 obtained from the U.S. Environmental Protection Agency  
556 ([https://aqs.epa.gov/aqsweb/airdata/download\\_files.html#Daily](https://aqs.epa.gov/aqsweb/airdata/download_files.html#Daily), last access: 1  
557 August 2022). The modeling results are made available at  
558 <https://doi.org/10.5281/zenodo.6891316> (last access: 1 August 2022).

559

## 560 **Acknowledgments**

561 HW acknowledges the support by the U.S. Department of Energy (DOE), Office  
562 of Science, Office of Biological and Environmental Research (BER), as part of  
563 the Earth and Environmental System Modeling program. The Pacific Northwest  
564 National Laboratory (PNNL) is operated for DOE by the Battelle Memorial  
565 Institute under contract DE-AC05-76RLO1830.

566

567 **Financial support.** This study was supported by the National Key Research  
568 and Development Program of China (grant 2020YFA0607803—~~and~~  
569 ~~2019YFA0606800~~), ~~the National Natural Science Foundation of China (grant~~  
570 ~~41975159)~~, ~~and~~, Jiangsu Science Fund for Distinguished Young Scholars  
571 (grant BK20211541) and the Jiangsu Science Fund for Carbon Neutrality (grant  
572 BK20220031).

573

---

574 **Competing interests.** The authors declare that they have no conflict of interest.  
575

---

## References

- 576  
577  
578 Atkinson, R.: Atmospheric chemistry of VOCs and NO<sub>x</sub>, *Atmos. Environ.*, 34,  
579 2063-2101, [https://doi.org/10.1016/S1352-2310\(99\)00460-4](https://doi.org/10.1016/S1352-2310(99)00460-4), 2000.
- 580  
581 Bates, K. H. and Jacob, D. J.: An Expanded Definition of the Odd Oxygen  
582 Family for Tropospheric Ozone Budgets: Implications for Ozone Lifetime and  
583 Stratospheric Influence, *Geophys. Res. Lett.*, 47, e2019GL084486,  
584 <https://doi.org/10.1029/2019gl084486>, 2020.
- 585  
586 Butler, T., Lupascu, A., and Nalam, A.: Attribution of ground-level ozone to  
587 anthropogenic and natural sources of nitrogen oxides and reactive carbon in a  
588 global chemical transport model, *Atmos. Chem. Phys.*, 20, 10707-10731,  
589 <https://doi.org/10.5194/acp-20-10707-2020>, 2020.
- 590  
591 Butler, T., Lupascu, A., Coates, J., and Zhu, a.-S.: TOAST 1.0: Tropospheric  
592 Ozone Attribution of Sources with Tagging for CESM 1.2.2, *Geosci. Model Dev.*,  
593 [11, 2825–2840](https://doi.org/10.5194/gmd-11-2825-2018), <https://doi.org/10.5194/gmd-11-2825-2018>, 2018.
- 594  
595 Castellanos, P. and Boersma, K. F.: Reductions in nitrogen oxides over Europe  
596 driven by environmental policy and economic recession, *Sci. Rep.*, 2, 265,  
597 <https://doi.org/10.1038/srep00265>, 2012.
- 598  
599 [Cheng, J., Tong, D., Liu, Y., Yu, S., Yan, L., Zheng, B., Geng, G., He, K., and](https://doi.org/10.1029/2021GL093197)  
600 [Zhang, Q.: Comparison of current and future PM<sub>2.5</sub> air quality in China under](https://doi.org/10.1029/2021GL093197)  
601 [CMIP6 and DPEC emission scenarios, \*Geophys. Res. Lett.\*, 48,](https://doi.org/10.1029/2021GL093197)  
602 [e2021GL093197, <https://doi.org/10.1029/2021GL093197>, 2021.](https://doi.org/10.1029/2021GL093197)
- 603  
604 Collet, S., Kidokoro, T., Karamchandani, P., Jung, J., and Shah, T.: Future year  
605 ozone source attribution modeling study using CMAQ-ISAM, *J&AWMA, Air*  
606 [Waste Manag. Assoc.](https://doi.org/10.1080/10962247.2018.1496954), 68, 1239-1247,  
607 <https://doi.org/10.1080/10962247.2018.1496954>, 2018.
- 608  
609 Cooper, O. R., Gao, R.-S., Tarasick, D., Leblanc, T., and Sweeney, C.: Long-  
610 term ozone trends at rural ozone monitoring sites across the United States,  
611 1990-2010, *J. Geophys. Res.: Atmospheres, Atmos.*, 117, D22307,  
612 <https://doi.org/10.1029/2012JD018261>, 2012.
- 613  
614 Cooper, O. R., Schultz, M. G., Schröder, S., Chang, K.-L., Gaudel, A., Gerardo,  
615 Benítez, C., Cuevas, E., Fröhlich, M., Galbally, I. E., Kubistin, D., Lu, X., Audra,  
616 McClure-Begley, A., Molloy, S., Nédélec, P., O'Brien, J., Oltmans, S. J., Irina,  
617 Petropavlovskikh, I., Ries, L., Senik, I., Sjöberg, K., Solberg, S., Spain, T. G.,



---

618 Spangl, W., Steinbacher, M., Tarasick, D., Thouret, V., and Xu, X.: Multi-decadal  
619 surface ozone trends at globally distributed remote locations, *Elem. Sci. Anth.*,  
620 8, 23, <https://doi.org/10.1525/elementa.420>, 2020.

621

622 Clappier, A., Belis, C. A., Pernigotti, D., and Thunis, P.: Source apportionment  
623 and sensitivity analysis: two methodologies with two different purposes, *Geosci.*  
624 *Model Dev.*, 10, 4245–4256, <https://doi.org/10.5194/gmd-10-4245-2017>, 2017.

625

626 ~~Crippa, M., Guizzardi, D., Muntean, M., Schaaf, E., Dentener, F., van Aardenne,~~  
627 ~~J. A., Monni, S., Doering, U., Olivier, J. G. J., Pagliari, V., and Janssens-~~  
628 ~~Maenhout, G.: Gridded emissions of air pollutants for the period 1970–2012~~  
629 ~~within EDGAR v4.3.2, *Earth Syst. Sci. Data*, 10, 1987–2013,~~  
630 ~~<https://doi.org/10.5194/essd-10-1987-2018>,~~  
631

632 ~~de Gouw, J. A., Parrish, D. D., Frost, G. J., and Trainer, M.: Reduced emissions~~  
633 ~~of CO<sub>2</sub>, NO<sub>x</sub>, and SO<sub>2</sub> from US power plants owing to switch from coal to~~  
634 ~~natural gas with combined cycle technology, *Earths Future*, 2, 75–82,~~  
635 ~~<https://doi.org/10.1002/2013EF000196>, 2014.~~

636

637 Duncan, B. N., Lamsal, L. N., Thompson, A. M., Yoshida, Y., Lu, Z., Streets, D.  
638 G., Hurwitz, M. M., and Pickering, K. E.: A space-based, high-resolution view of  
639 notable changes in urban NO<sub>x</sub> pollution around the world (2005–2014), *J. J.*  
640 *Geophys. Res. Atmos.*, 21, 976–996, <https://doi.org/10.1002/2015JD024121>,  
641 2016.

642

643 ~~Duncan, B. N., Yoshida, Y., de Foy, B., Lamsal, L. N., Streets, D. G., Lu, Z.,~~  
644 ~~Pickering, K. E., and Krotkov, N. A.: The observed response of Ozone~~  
645 ~~Monitoring Instrument (OMI) NO<sub>2</sub> columns to NO<sub>x</sub> emission controls on power~~  
646 ~~plants in the United States: 2005–2011, *Atmos. Environ.*, 81, 102–111,~~  
647 ~~<https://doi.org/10.1016/j.atmosenv.2013.08.068>, 2013.~~

648

649 Dunker, A. M., Yarwood, G., Ortmann, J. P., and Wilson, G. M.: Comparison of  
650 Source Apportionment and Source Sensitivity of Ozone in a Three-Dimensional  
651 Air Quality Model, *Environ. Sci. Technol.*, 36, 2953–2964,  
652 <https://doi.org/10.1021/es011418f>, 2002.

653

654 ~~EIA: US Energy Information Administration: Drilling Productivity Report,~~  
655 ~~available at: <https://www.eia.gov/petroleum/drilling/>, last access: 7 April 2020.~~

656

657 Emmons, L. K., Hess, P. G., Lamarque, J.-F., and Pfister, G. G.: Tagged ozone  
658 mechanism for MOZART-4, CAM-chem and other chemical transport models,  
659 *Geosci. Model Dev.*, 5, 1531–1542, <https://doi.org/10.5194/gmd-5-1531-2012>,

---

660 2012.  
661  
662 Emmons, L. K., Walters, S., Hess, P. G., Lamarque, J.-F., Pfister, G. G., Fillmore,  
663 D., Granier, C., Guenther, A., Kinnison, D., Laepple, T., Orlando, J., Tie, X.,  
664 Tyndall, G., Wiedinmyer, C., Baughcum, S. L., and Kloster, S.: Description and  
665 evaluation of the Model for Ozone and Related chemical Tracers, version 4  
666 (MOZART-4), *Geosci. Model Dev.*, 3, 43–67, [https://doi.org/10.5194/gmd-3-43-](https://doi.org/10.5194/gmd-3-43-2010)  
667 2010, 2010.  
668  
669 Eyring, V., [Köhler, H. W., van Aardenne, J., and Lauer, A.](#): Emissions from  
670 international shipping: 1. The last 50 years, *J. Geophys. Res.*, 110, [D17305](#),  
671 <https://doi.org/10.1029/2004JD005619>, 2005.  
672  
673 [Fan, T., Liu, X., Ma, P.-L., Zhang, Q., Li, Z., Jiang, Y., Zhang, F., Zhao, C., Yang,](#)  
674 [X., Wu, F., and Wang, Y.](#): Emission or atmospheric processes? An attempt to  
675 [attribute the source of large bias of aerosols in eastern China simulated by](#)  
676 [global climate models](#), *Atmos. Chem. Phys.*, 18, 1395–1417,  
677 <https://doi.org/10.5194/acp-18-1395-2018>, 2018.  
678  
679 Fiore, A. M., West, J. J., Horowitz, L. W., Naik, V., and Schwarzkopf, M. D.:  
680 Characterizing the tropospheric ozone response to methane emission controls  
681 and the benefits to climate and air quality, *J. Geophys. Res.*, 113, D08307,  
682 <https://doi.org/10.1029/2007JD009162>, 2008.  
683  
684 Fiore, A. M., Dentener, F. J., Wild, O., Cuvelier, C., Schultz, M. G., Hess, P.,  
685 Textor, C., Schulz, M., Doherty, R. M., Horowitz, L. W., MacKenzie, I. A.,  
686 Sanderson, M. G., Shindell, D. T., Stevenson, D. S., Szopa, S., van Dingenen,  
687 R., Zeng, G., Atherton, C., Bergmann, D., Bey, I., Carmichael, G., Collins, W. J.,  
688 Duncan, B. N., Faluvegi, G., Folberth, G., Gauss, M., Gong, S., Hauglustaine,  
689 D., Holloway, T., Isaksen, I. S. A., Jacob, D. J., Jonson, J. E., Kaminski, J. W.,  
690 Keating, T. J., Lupu, A., Marmer, E., Montanaro, V., Park, R. J., Pitari, G., Pringle,  
691 K. J., Pyle, J. A., Schroeder, S., Vivanco, M. G., Wind, P., Wojcik, G., Wu, S.,  
692 and Zuber, A.: Multimodel estimates of intercontinental source-receptor  
693 relationships for ozone pollution, *J. Geophys. Res.*, 114, D04301 ,  
694 <https://doi.org/10.1029/2008JD010816>, 2009.  
695  
696 Fleming, Z. L., Doherty, R. M., Schneidemesser, E. V., Malley, C. S., Cooper,  
697 O. R., Pinto, J. P., Colette, A., Xu, X., Simpson, D., Schultz, M. G., Lefohn, A.  
698 S., Hamad, S., Moolla, R., Solberg, S., and Feng, Z.: Tropospheric Ozone  
699 Assessment Report: Present-day ozone distribution and trends relevant to  
700 human health, *Elem. Sci. Anth.*, 6, [p-12](#), <https://doi.org/10.1525/elementa.273>,  
701 2018.

702

703 Gao, J., Zhu, B., Xiao, H., Kang, H., Hou, X., and Shao, P.: A case study of  
704 surface ozone source apportionment during a high concentration episode,  
705 under frequent shifting wind conditions over the Yangtze River Delta, China, *Sci.*  
706 *Total Environ.*, 544, 853-863, <https://doi.org/10.1016/j.scitotenv.2015.12.039>,  
707 2016.

708

709 Gao, Y., Fu, J. S., Drake, J. B., Lamarque, J. F., and Liu, Y.: The impact of  
710 emission and climate change on ozone in the United States under  
711 representative concentration pathways (RCPs), *Atmos. Chem. Phys.*, 13, 9607-  
712 9621, <https://doi.org/10.5194/acp-13-9607-2013>, 2013.

713

714 Gaudel, A., Cooper, O. R. , Chang, K. L., Bourgeois, I., Ziemke, J. R., Strode,  
715 S. A., Oman, L. D., Sellitto, P., Nédélec, P., Bolt, R., Thouret, V. and Granier, C.:  
716 Aircraft observations since the 1990s reveal increases of tropospheric ozone at  
717 multiple locations across the Northern Hemisphere, *Sci. AdvanceAdv.*, 6,  
718 [eaba8272](https://doi.org/10.1126/sciadv.aba8272), <https://doi.org/10.1126/sciadv.aba8272>, 2020.

719

720 Gelaro, R., McCarty, W., Suárez, M. J., Todling, R., Molod, A., Takacs, L.,  
721 Randles, C. A., Darmenov, A., Bosilovich, M. G., Re- iche, R., Wargan, K., Coy,  
722 L., Cullather, R., Draper, C., Akella, S., Buchard, V., Conaty, A., da Silva, A. M.,  
723 Gu, W., Kim, G., Koster, R., Lucchesi, R., Merkova, D., Nielsen, J. E., Partyka,  
724 G., Pawson, S., Putman, W., Rienecker, M., Schubert, S. D., Sienkiewicz, M.,  
725 and Zhao, B.: The Modern-Era Retrospective Analysis for Research and  
726 Applications, Version 2 (MERRA-2), *J. Climate*, 30, 5419–5454,  
727 <https://doi.org/10.1175/JCLI-D-16-0758.1>, 2017.

728

729 [Grewe, V., Tsati, E., Mertens, M., Frömming, C., and Jöckel, P.: Contribution of](https://doi.org/10.5194/gmd-10-2615-2017)  
730 [emissions to concentrations: the TAGGING 1.0 submodel based on the](https://doi.org/10.5194/gmd-10-2615-2017)  
731 [Modular Earth Submodel System \(MESSy 2.52\)](https://doi.org/10.5194/gmd-10-2615-2017), *Geosci. Model Dev.*, 10,  
732 [2615–2633](https://doi.org/10.5194/gmd-10-2615-2017), <https://doi.org/10.5194/gmd-10-2615-2017>, 2017.

733

734 Haagen-Smit, A. J.: Chemistry and Physiology of Los Angeles Smog, *Ind. Eng.*  
735 *Chem.*, 44, 1342-1346, <https://doi.org/10.1021/ie50510a045>, 1952.

736

737 Hodnebrog, Ø., Berntsen, T. K., Dessens, O., Gauss, M., Grewe, V., Isaksen, I.  
738 S. A., Koffi, B., Myhre, G., Olivié, D., Prather, M. J., Pyle, J. A., Stordal, F., Szopa,  
739 S., Tang, Q., van Velthoven, P., Williams, J. E., and Ødemark, K.: Future impact  
740 of non-land based traffic emissions on atmospheric ozone and OH – an  
741 optimistic scenario and a possible mitigation strategy, *Atmos. Chem. Phys.*, 11,  
742 11293–11317, <https://doi.org/10.5194/acp-11-11293-2011>, 2011.

743

---

744 Hoesly, R. M., Smith, S. J., Feng, L., Klimont, Z., Janssens-Maenhout, G.,  
745 Pitkanen, T., Seibert, J. J., Vu, L., Andres, R. J., Bolt, R. M., Bond, T. C.,  
746 Dawidowski, L., Kholod, N., Kurokawa, J.-I., Li, M., Liu, L., Lu, Z., Moura, M. C.  
747 P., O'Rourke, P. R., and Zhang, Q.: Historical (1750–2014) anthropogenic  
748 emissions of reactive gases and aerosols from the Community Emissions Data  
749 System (CEDS), *Geosci. Model Dev.*, 11, 369–408,  
750 <https://doi.org/10.5194/gmd-11-369-2018>, 2018.

751

752 Han, H., Liu, J., Yuan, H., Zhuang, B., Zhu, Y., Wu, Y., Yan, Y., and Ding, A.:  
753 Characteristics of intercontinental transport of tropospheric ozone from Africa  
754 to Asia, *Atmos. Chem. Phys.*, 18, 4251–4276, [https://doi.org/10.5194/acp-18-](https://doi.org/10.5194/acp-18-4251-2018)  
755 [4251-2018](https://doi.org/10.5194/acp-18-4251-2018), 2018.

756

757 Hoor, P., Borken-Kleefeld, J., Caro, D., Dessens, O., Endresen, Ø., Gauss, M.,  
758 Grewe, V., Hauglustaine, D. A., Isaksen, I. S. A., Jöckel, P., Lelieveld, J., Myhre,  
759 G., Meijer, E. W., Olivie, D., Prather, M. J., Poberaj, C. S., Shine, K. P., Staehelin,  
760 J., Tang, Q., Aardenne, J. v., Velthoven, P. F. J. v., and Sausen, R.: The impact  
761 of traffic emissions on atmospheric ozone and OH: results from QUANTIFY,  
762 *Atmos. Chem. Phys.*, 9, 3113–3116, <https://doi.org/10.5194/acp-9-3113-2009>,  
763 2009.

764

765 ~~[Jaffe, D. A., Cooper, O. R., Fiore, A. M., Henderson, B. H., Tonnesen, G. S.,](#)~~  
766 ~~[Russell, A. G., Henze, D. K., Langford, A. O., Lin, M., and Moore, T.: Scientific](#)~~  
767 ~~[assessment of background ozone over the U.S.: Implications for air quality](#)~~  
768 ~~[management, \*Elem. Sci.\* Jaffe, D. A., Cooper, O. R., Fiore, A. M., Henderson,](#)~~  
769 ~~[B. H., Tonnesen, G. S., Russell, A. G., Henze, D. K., Langford, A. O., Lin, M.,](#)~~  
770 ~~[and Moore, T.: Scientific assessment of background ozone over the U.S.:](#)~~  
771 ~~[Implications for air quality management, \*Elem. Sci. Anth.\*, 6, 56, doi:](#)~~  
772 ~~<https://doi.org/10.1525/elementa.309>, 2018.~~  
773 ~~[Anth, 6, 56, https://doi.org/ https://doi.org/10.1525/elementa.309](https://doi.org/), 2018.~~

774

775 Johnson, C., Collins, W., Stevenson, D., and Derwent, R.: Relative roles of  
776 climate and emissions changes on future tropospheric oxidant concentrations,  
777 *J. Geophys. Res.-Atmos.*, 104, 18631–18645,  
778 <https://doi.org/10.1029/1999JD900204>, 1999.

779

780 Kasibhatla, P., Levy, H., Moxim, W. J., Pandis, S. N., Corbett, J. J., Peterson,  
781 M. C., Honrath, R. E., Frost, G. J., Knapp, K., Parrish, D. D., and Ryerson, T.  
782 B.: Do emissions from ships have a significant impact on concentrations of  
783 nitrogen oxides in the marine boundary layer?, *Geophys. Res. Lett.*, 27, 2229–  
784 2232, <https://doi.org/10.1029/2000gl011387>, 2000.

785

---

786 Koo, B., Wilson, G. M., Morris, R., Dunker, A. M., and Yarwood, G.: Comparison  
787 of Source Apportionment and Sensitivity Analysis in a Particulate Matter Air  
788 Quality Model, *Environ. Sci. Technol.*, 43, 6669–6675,  
789 <https://doi.org/10.1021/es9008129>, 2009.

790

~~791 Krotkov, N. A., McLinden, C. A., Li, C., Lamsal, L. N., Celarier, E. A., Marchenko,  
792 S. V., Swartz, W. H., Bucsela, E. J., Joiner, J., Duncan, B. N., Boersma, K. F.,  
793 Veefkind, J. P., Levelt, P. F., Fioletov, V. E., Dickerson, R. R., He, H., Lu, Z.,  
794 and Streets, D. G.: Aura OMI observations of regional SO<sub>2</sub> and NO<sub>2</sub> pollution  
795 changes from 2005 to 2015, *Atmos. Chem. Phys.*, 16, 4605–4629,  
796 <https://doi.org/10.5194/acp-16-4605-2016>, 2016.~~

797

798 Kwok, R. H. F., Baker, K. R., Napelenok, S. L., and Tonnesen, G. S.:  
799 Photochemical grid model implementation and application of VOC, NO<sub>x</sub>, and  
800 O<sub>3</sub> source apportionment, *Geosci. Model Dev.*, 8, 99–114,  
801 <https://doi.org/10.5194/gmd-8-99-2015>, 2015.

802

803 Lamarque, J.-F., Emmons, L. K., Hess, P. G., Kinnison, D. E., Tilmes, S., Vitt,  
804 F., Heald, C. L., Holland, E. A., Lauritzen, P. H., Neu, J., Orlando, J. J., Rasch,  
805 P. J., and Tyndall, G. K.: CAM-chem: description and evaluation of interactive  
806 atmospheric chemistry in the Community Earth System Model, *Geosci. Model  
807 Dev.*, 5, 369–411, <https://doi.org/10.5194/gmd-5-369-2012>, 2012.

808

809 Lin, M., Fiore, A. M., Horowitz, L. W., Langford, A. O., Oltmans, S. J., Tarasick,  
810 D., and Rieder, H. E.: Climate variability modulates western U.S. ozone air  
811 quality in spring via deep stratospheric intrusions, *Nat. Commun.*, 6, 7105,  
812 <https://doi.org/10.1038/ncomms8105>, 2015.

813

814 Lin, M., Horowitz, L. W., Payton, R., Fiore, A. M., and Tonnesen, G. S.: US  
815 surface ozone trends and extremes from 1980 to 2014: quantifying the roles of  
816 rising Asian emissions, domestic controls, wildfires, and climate, *Atmos. Chem.  
817 Phys.*, 17, 2943–2970, <https://doi.org/10.5194/acp-17-2943-2017>, 2017.

818

~~819 Lin, M., Fiore, A. M., Cooper, O. R., Horowitz, L. W., Langford, A. O., Levy, H.,  
820 Johnson, B. J., Naik, V., Oltmans, S. J., and Senff, C. J.: Springtime high  
821 surface ozone events over the western United States: Quantifying the role of  
822 stratospheric intrusions, *J. Geophys. Res. Atmos.*, 117,  
823 <https://doi.org/10.1029/2012JD018151>, 2012.~~

824

825 Lupaşcu, A. and Butler, T.: Source attribution of European surface O<sub>3</sub> using a  
826 tagged O<sub>3</sub> mechanism, *Atmos. Chem. Phys.*, 19, 14535–14558,  
827 <https://doi.org/10.5194/acp-19-14535-2019>, 2019.

828

829 Mertens, M., Kerkweg, A., Grewe, V., Jöckel, P., and Sausen, R.: Attributing  
830 ozone and its precursors to land transport emissions in Europe and Germany,  
831 *Atmos. Chem. Phys.*, 20, 7843–7873, [https://doi.org/10.5194/acp-20-7843-](https://doi.org/10.5194/acp-20-7843-2020)  
832 2020, 2020.

833

834 McDuffie, E. E., Smith, S. J., O'Rourke, P., Tibrewal, K., Venkataraman, C.,  
835 Marais, E. A., Zheng, B., Crippa, M., Brauer, M., and Martin, R. V.: A global  
836 anthropogenic emission inventory of atmospheric pollutants from sector- and  
837 fuel-specific sources (1970–2017): an application of the Community Emissions  
838 Data System (CEDs), *Earth Syst. Sci. Data*, 12, 3413–3442,  
839 <https://doi.org/10.5194/essd-12-3413-2020>, 2020.

840

841 Müller-Casseres, E., Edelenbosch, O. Y., Szklo, A., Schaeffer, R., and van  
842 Vuuren, D. P.: Global futures of trade impacting the challenge to decarbonize  
843 the international shipping sector, *Energy*, 237, 121547,  
844 <https://doi.org/10.1016/j.energy.2021.121547>, 2021

845

846 Myhre, G., D. Shindell, F.-M. Bréon, W. Collins, J. Fuglestvedt, J. Huang, D.  
847 Koch, J.-F. Lamarque, D. Lee, B. Mendoza, T. Nakajima, A. Robock, G.  
848 Stephens, T. Takemura and H. Zhang, 2013: Anthropogenic and Natural  
849 Radiative Forcing. In: *Climate Change 2013: The Physical Science Basis.*  
850 Contribution of Working Group I to the Fifth Assessment Report of the  
851 Intergovernmental Panel on Climate Change [Stocker, T.F., D. Qin, G.-K.  
852 Plattner, M. Tignor, S.K. Allen, J. Boschung, A. Nauels, Y. Xia, V. Bex and P.M.  
853 Midgley (eds.)]. Cambridge University Press, Cambridge, United Kingdom and  
854 New York, NY, USA, 2013.

855

856 [Price, C., Penner, J., and Prather, M.: NO<sub>x</sub> from lightning 1. Global distribution](https://doi.org/10.1029/96JD03504)  
857 [based on lightning physics, \*J. Geophys. Res.\*, 102, 5929–5941,](https://doi.org/10.1029/96JD03504)  
858 <https://doi.org/10.1029/96JD03504>, 1997.

859

860 O'Neill, B. C., Tebaldi, C., van Vuuren, D. P., Eyring, V., Friedlingstein, P., Hurtt,  
861 G., Knutti, R., Kriegler, E., Lamarque, J.-F., Lowe, J., Meehl, G. A., Moss, R.,  
862 Riahi, K., and Sanderson, B. M.: The Scenario Model Intercomparison Project  
863 (ScenarioMIP) for CMIP6, *Geosci. Model Dev.*, 9, 3461–3482,  
864 <https://doi.org/10.5194/gmd-9-3461-2016>, 2016.

865

866 ~~[Price, C., Penner, J., and Prather, M.: NO<sub>x</sub> from lightning 1. Global distribution](https://doi.org/10.1029/96JD03504)~~  
867 ~~[based on lightning physics, \*J. Geophys. Res.\*, 102, 5929–5941,](https://doi.org/10.1029/96JD03504)~~  
868 ~~<https://doi.org/10.1029/96JD03504>, 1997.~~

869



---

870 Seinfeld, J. H. and Pandis, S. N.: Atmospheric Chemistry and Physics: From  
871 Air Pollution to Climate Change, J. Wiley, Hoboken, N.J., 2006.  
872

873 Simon, H., Reff, A., Wells, B., Xing, J., and Frank, N.: Ozone trends across the  
874 United States over a period of decreasing NO<sub>x</sub> and VOC emissions, Environ.  
875 Sci. Technol., 49, 186-195, <https://doi.org/10.1021/es504514z>, 2015.  
876

877 Shen, L. and Mickley, L. J.: Effects of El Niño on summertime ozone air quality  
878 in the eastern United States, Geophys. Res. Lett., 44, 12543–~~50~~[12550](https://doi.org/10.1029/2017GL076150),  
879 <https://doi.org/10.1029/2017GL076150>, 2017.  
880

881 Stevenson, D. S., Dentener, F. J., Schultz, M. G., Ellingsen, K., van Noije, T. P.  
882 C., Wild, O., Zeng, G., Amann, M., Atherton, C. S., Bell, N., Bergmann, D. J.,  
883 Bey, I., Butler, T., Cofala, J., Collins, W. J., Derwent, R. G., Doherty, R. M.,  
884 Drevet, J., Eskes, H. J., Fiore, A. M., Gauss, M., Hauglustaine, D. A., Horowitz,  
885 L. W., Isaksen, I. S. A., Krol, M. C., Lamarque, J.-F., Lawrence, M. G.,  
886 Montanaro, V., Müller, J.-F., Pitari, G., Prather, M. J., Pyle, J. A., Rast, S.,  
887 Rodriguez, J. M., Sanderson, M. G., Savage, N. H., Shindell, D. T., Strahan, S.  
888 E., Sudo, K., and Szopa, S.: Multimodel ensemble simulations of present-day  
889 and near-future tropospheric ozone, J. Geophys. Res., 111, D08301.  
890 <https://doi.org/10.1029/2005JD006338>, 2006.  
891

892 Sudo, K., and Akimoto, H.: Global source attribution of tropospheric ozone:  
893 Long-range transport from various source regions, J. Geophys. Res., 112,  
894 D12302, <https://doi.org/10.1029/2006JD007992>, 2007.  
895

896 Szopa, S., ~~V.~~Naik, ~~B.V.~~Adhikary, ~~P.B.~~Artaxo, ~~T.P.~~Berntsen, ~~W.D.T.~~Collins,  
897 ~~S.W.D.~~Fuzzi, ~~L.S.~~Gallardo, ~~A.L.~~Kiendler-Scharr, ~~Z.A.~~Klimont, ~~H.Z.~~Liao,  
898 ~~N.H.~~Unger, ~~N.~~ and ~~P.~~Zanis, ~~P.~~, 2021: Short-Lived Climate Forcers. In  
899 Climate Change 2021: The Physical Science Basis. Contribution of Working  
900 Group I to the Sixth Assessment Report of the Intergovernmental Panel on  
901 Climate Change [Masson-Delmotte, V., ~~P.~~Zhai, ~~A.P.~~Pirani, ~~S.L.A.~~Connors,  
902 ~~C.S.L.~~Péan, ~~S.C.~~Berger, ~~N.S.~~Caud, ~~Y.N.~~Chen, ~~L.Y.~~Goldfarb, ~~M.H.L.~~  
903 Gomis, M., ~~I.~~Huang, ~~K.M.~~Leitzell, ~~E.K.~~Lonnoy, ~~J.B.R.E.~~Matthews, ~~T.K.~~  
904 ~~J.B.R.~~Maycock, ~~T.K.~~Waterfield, ~~O.T.~~Yelekçi, ~~R.O.~~Yu, ~~R.~~ and ~~B.~~Zhou ~~B.~~  
905 (eds.)]. Cambridge University Press, Cambridge, United Kingdom and New  
906 York, NY, USA, pp. 817–922, <https://doi.org/10.1017/9781009157896.008>,  
907 2021.  
908

909 Thor, R. N., Mertens, M., Matthes, S., Righi, M., Hendricks, J., Brinkop, S., Graf,  
910 P., Grewe, V., Jöckel, P., and Smith, S.: An inconsistency in aviation emissions  
911 between CMIP5 and CMIP6 and the implications for short-lived species and

---

912 their radiative forcing, *Geosci. Model Dev.*, 16, 1459–1466,  
913 <https://doi.org/10.5194/gmd-16-1459-2023>, 2023.

914

915 Thunis, P., Clappier, A., Tarrason, L., Cuvelier, C., Monteiro, A., Pisoni, E.,  
916 Wesseling, J., Belis, C., Pirovano, G., Janssen, S., Guerreiro, C., and Peduzzi,  
917 E.: Source apportionment to support air quality planning: Strengths and  
918 weaknesses of existing approaches, *Environ. Int.*, 130, 104825,  
919 <https://doi.org/10.1016/j.envint.2019.05.019>, 2019.

920

921 Tilmes, S., Lamarque, J. F., Emmons, L. K., Kinnison, D. E., Marsh, D., Garcia,  
922 R. R., Smith, A. K., Neely, R. R., Conley, A., Vitt, F., Val Martin, M., Tanimoto,  
923 H., Simpson, I., Blake, D. R., and Blake, N.: Representation of the Community  
924 Earth System Model (CESM1) CAM4-chem within the Chemistry-Climate  
925 Model Initiative (CCMI), *Geosci. Model Dev.*, 9, 1853–1890,  
926 <https://doi.org/10.5194/gmd-9-1853-2016>, 2016.

927

928 Tilmes, S., Lamarque, J. F., Emmons, L. K., Kinnison, D. E., Ma, P. L., Liu, X.,  
929 Ghan, S., Bardeen, C., Arnold, S., Deeter, M., Vitt, F., Ryerson, T., Elkins, J. W.,  
930 Moore, F., Spackman, J. R., and Val Martin, M.: Description and evaluation of  
931 tropospheric chemistry and aerosols in the Community Earth System Model  
932 (CESM1.2), *Geosci. Model Dev.*, 8, 1395–1426, [https://doi.org/10.5194/gmd-8-](https://doi.org/10.5194/gmd-8-1395-2015)  
933 [1395-2015](https://doi.org/10.5194/gmd-8-1395-2015), 2015.

934

935 ~~Tilmes, S., Lamarque, J. F., Emmons, L. K., Kinnison, D. E., Ma, P. L., Liu, X.,~~  
936 ~~Ghan, S., Bardeen, C., Arnold, S., Deeter, M., Vitt, F., Ryerson, T., Elkins, J. W.,~~  
937 ~~Moore, F., Spackman, J. R., and Val Martin, M.: Description and evaluation of~~  
938 ~~tropospheric chemistry and aerosols in the Community Earth System Model~~  
939 ~~(CESM1.2), *Geosci. Model Dev.*, 8, 1395–1426, [https://doi.org/10.5194/gmd-8-](https://doi.org/10.5194/gmd-8-1395-2015)~~  
940 ~~[1395-2015](https://doi.org/10.5194/gmd-8-1395-2015), 2015.~~

941

942 van Marle, M. J. E., Kloster, S., Magi, B. I., Marlon, J. R., Daniau, A.-L., Field,  
943 R. D., Arneth, A., Forrest, M., Hantson, S., Kehrwald, N. M., Knorr, W., Lasslop,  
944 G., Li, F., Mangeon, S., Yue, C., Kaiser, J. W., and van der Werf, G. R.: Historic  
945 global biomass burning emissions for CMIP6 (BB4CMIP) based on merging  
946 satellite observations with proxies and fire models (1750–2015), *Geosci. Model*  
947 *Dev.*, 10, 3329–3357, <https://doi.org/10.5194/gmd-10-3329-2017>, 2017.

948

949 von Glasow, R., Lawrence, M. G., Sander, R., and Crutzen, P. J.: Modeling the  
950 chemical effects of ship exhaust in the [cloudfreecloud-free](#) marine boundary  
951 layer, *Atmos. Chem. Phys.*, 3, 233–250, [https://doi.org/10.5194/acp-3-233-](https://doi.org/10.5194/acp-3-233-2003)  
952 [2003](https://doi.org/10.5194/acp-3-233-2003), 2003.

953



---

954 Wang, H., Rasch, P. J., Easter, R. C., Singh, B., Zhang, R., Ma, P.-L., Qian, Y.,  
955 Ghan, S. J., and Beagley, N.: Using an explicit emission tagging method in  
956 global modeling of source-receptor relationships for black carbon in the Arctic:  
957 Variations, sources, and transport pathways, *J. Geophys. Res. Atmos.*, 119,  
958 12888-12909, <https://doi.org/10.1002/2014JD022297>, 2014.  
959

960 Wesely, M. L.: Parameterizations for surface resistance to gaseous dry  
961 deposition in regional-scale numerical models, *Atmos. Environ.*, 23, 1293–1304,  
962 [https://doi.org/10.1016/0004-6981\(89\)90153-4](https://doi.org/10.1016/0004-6981(89)90153-4), 1989.  
963

964 Xing, J., Pleim, J. E., Mathur, R., Pouliot, G., Hogrefe, C., Gan, C.-M., and Wei,  
965 C.: Historical gaseous and primary aerosol emissions in the United States from  
966 1990 to 2010, *Atmos. Chem. Phys.*, 13, 7531–7549,  
967 <https://doi.org/10.5194/acp-13-7531-2013>, 2013.  
968

969 Yang, Y., Li, M., Wang, H., Li, H., Wang, P., Li, K., Gao, M., and Liao, H.: ENSO  
970 modulation of summertime tropospheric ozone over China, *Environ. Res. Lett.*,  
971 17, 034020, <https://doi.org/10.1088/1748-9326/ac54cd>, 2022.  
972

973 Yang, Y., Liao, H., and Li, J.: Impacts of the East Asian summer monsoon on  
974 interannual variations of summertime surface-layer ozone concentrations over  
975 China, *Atmos. Chem. Phys.*, 14, 6867–6879, <https://doi.org/10.5194/acp-14-6867-2014>, 2014.  
976

977

978 Yang, Y., Wang, H., Smith, S. J., Zhang, R., Lou, S., Yu, H., Li, C., and Rasch,  
979 P. J.: Source apportionments of aerosols and their direct radiative forcing and  
980 long-term trends over continental United States, *Earth's Future*, 6, 793–808,  
981 <https://doi.org/10.1029/2018EF000859>, 2018.  
982

983 Zhang, L., Jacob, D. J., Boersma, K. F., Jaffe, D. A., Olson, J. R., Bowman, K.  
984 W., Worden, J. R., Thompson, A. M., Avery, M. A., Cohen, R. C., Dibb, J. E.,  
985 Flock, F. M., Fuelberg, H. E., Huey, L. G., McMillan, W. W., Singh, H. B., and  
986 Weinheimer, A. J.: Transpacific transport of ozone pollution and the effect of  
987 recent Asian emission increases on air quality in North America: an integrated  
988 analysis using satellite, aircraft, ozonesonde, and surface observations, *Atmos.*  
989 *Chem. Phys.*, 8, 6117–6136, <https://doi.org/10.5194/acp-8-6117-2008>, 2008.  
990

991 Zhang, Y., Cooper, O. R., Gaudel, A., Nedelec, P., Ogino, S. Y., Thompson, A.  
992 M., and West, J. J.: Tropospheric ozone change from 1980 to 2010 dominated  
993 by equatorward redistribution of emissions, *Nat. Geosci.*, 9, 875-879,  
994 <https://doi.org/10.1038/ngeo2827>, 2016.  
995

---

996 Zhang, Y., West, J. J., Emmons, L. K., Flemming, J., Jonson, J. E., Lund, M. T.,  
997 Sekiya, T., Sudo, K., Gaudel, A., Chang, K. L., Nédélec, P., and Thouret, V.:  
998 Contributions of World Regions to the Global Tropospheric Ozone Burden  
999 Change From 1980 to 2010, *Geophys. Res. Lett.*, 48, [e2020GL089184](https://doi.org/10.1029/2020GL089184),  
1000 <https://doi.org/10.1029/2020GL089184>, 2021.

1001  
1002  
1003  
1004  
  
1005  
1006  
1007

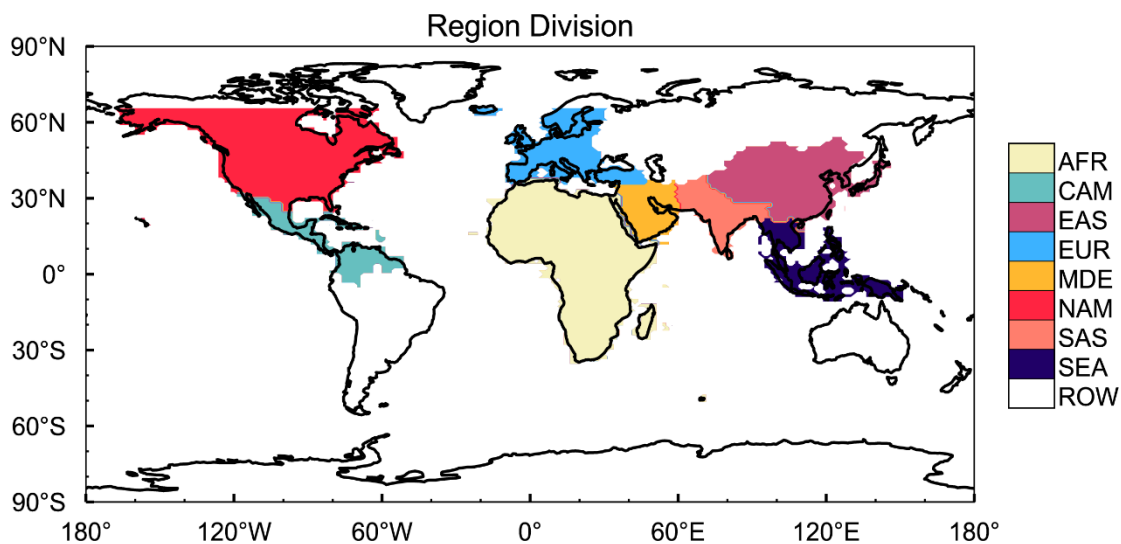
---

**Table 1.** O<sub>3</sub> trends (ppb/decade) over eastern U.S. and western U.S. in winter (December-January-February, DJF) and summer (June-July-August, JJA) from observations and model simulations.

---

<u>Season</u>	<u>Source</u>	<u>eastern U.S.</u>	<u>western U.S.</u>
<u>DJF</u>	<u>Observation</u>	<u>2.1 ± 0.29</u>	<u>2.2 ± 0.23</u>
<u>DJF</u>	<u>Model</u>	<u>6.1 ± 0.40</u>	<u>3.2 ± 0.28</u>
<u>JJA</u>	<u>Observation</u>	<u>-3.0±0.41</u>	<u>-0.5 ± 0.42</u>
<u>JJA</u>	<u>Model</u>	<u>-3.0±0.29</u>	<u>-2.3 ± 0.20</u>

---

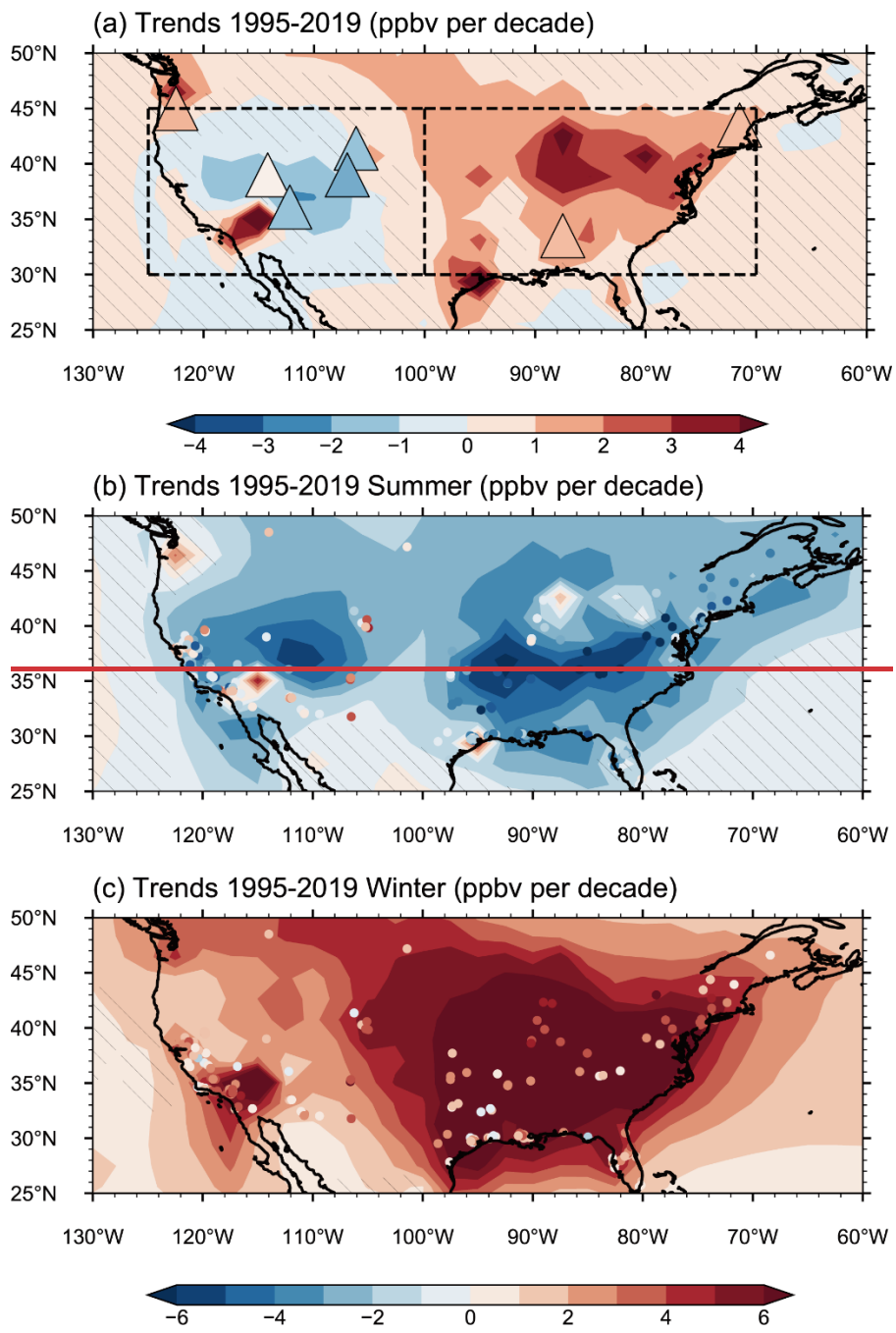


1008

1009

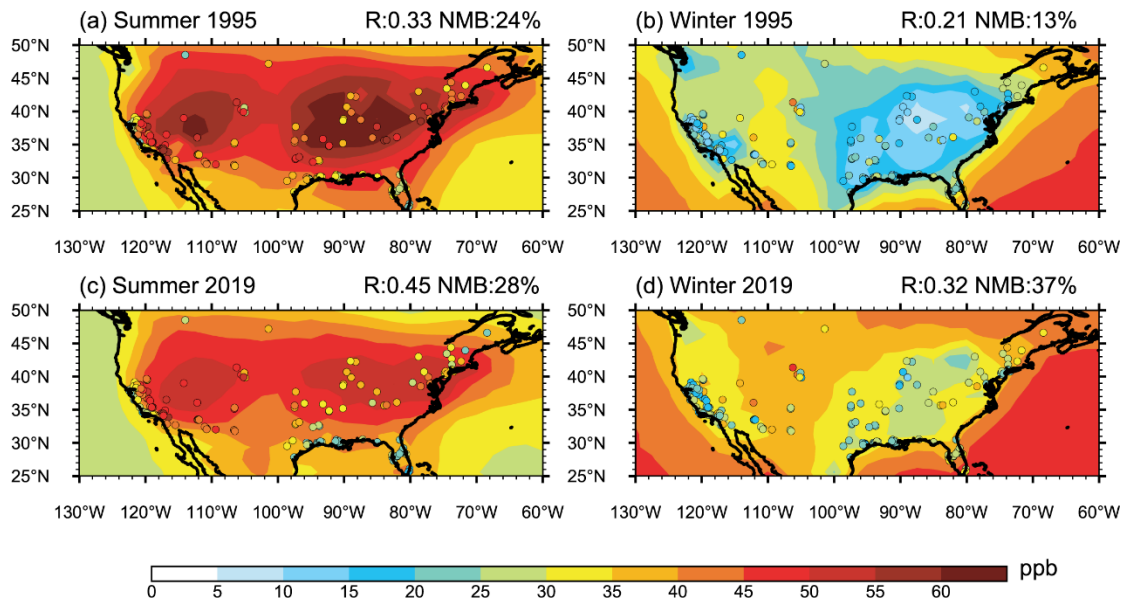
1010 **Figure 1.** Source regions that are selected for O<sub>3</sub> source tagging in this study,  
1011 include Africa (AFR), Central America (CAM), East Asia (EAS), Europe (EUR),  
1012 Middle East (MDE), North America (NAM), South Asia (SAS), Southeast Asia  
1013 (SEA) and rest of the world (ROW).

1014



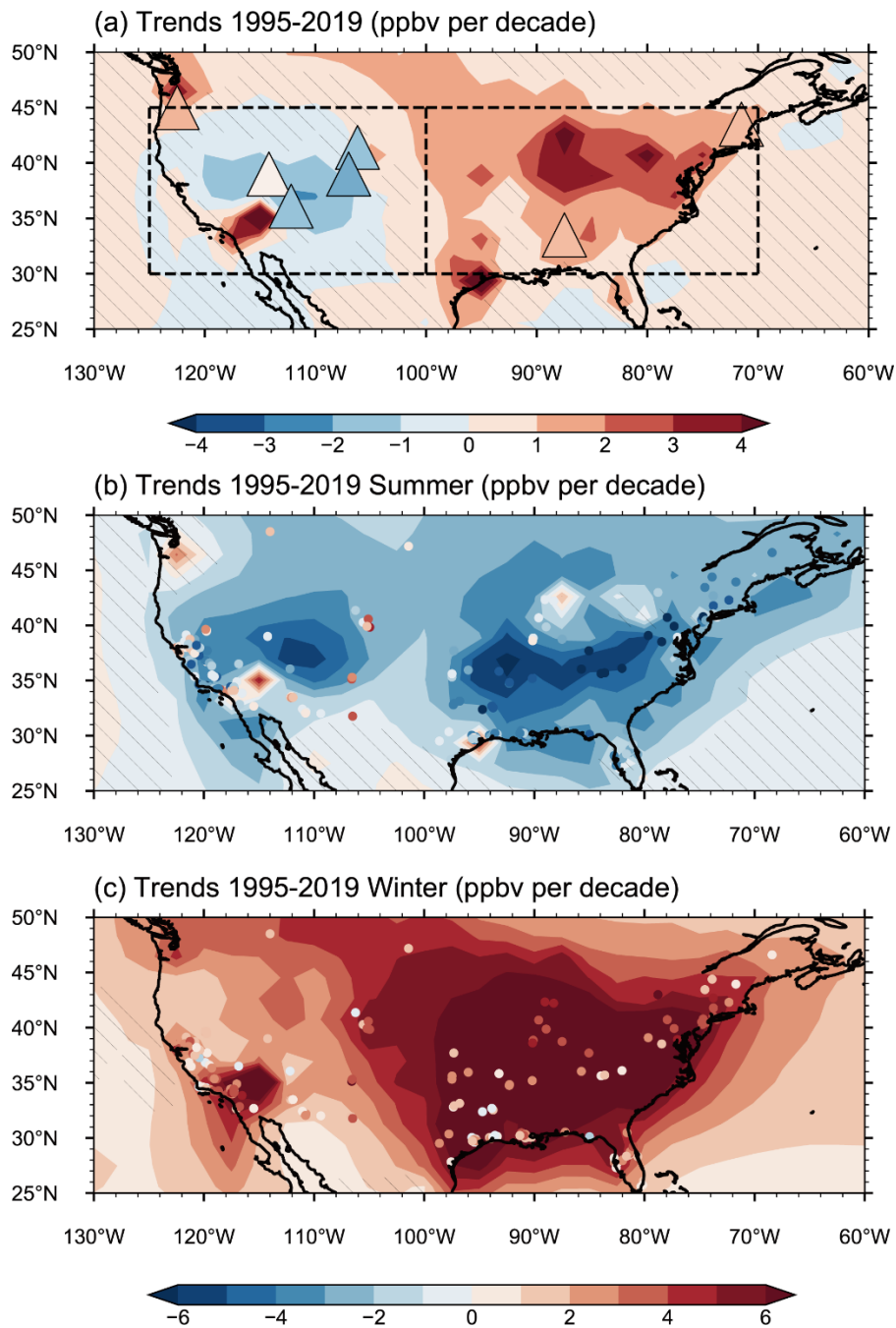
1015  
 1016  
 1017

**Figure 2.**



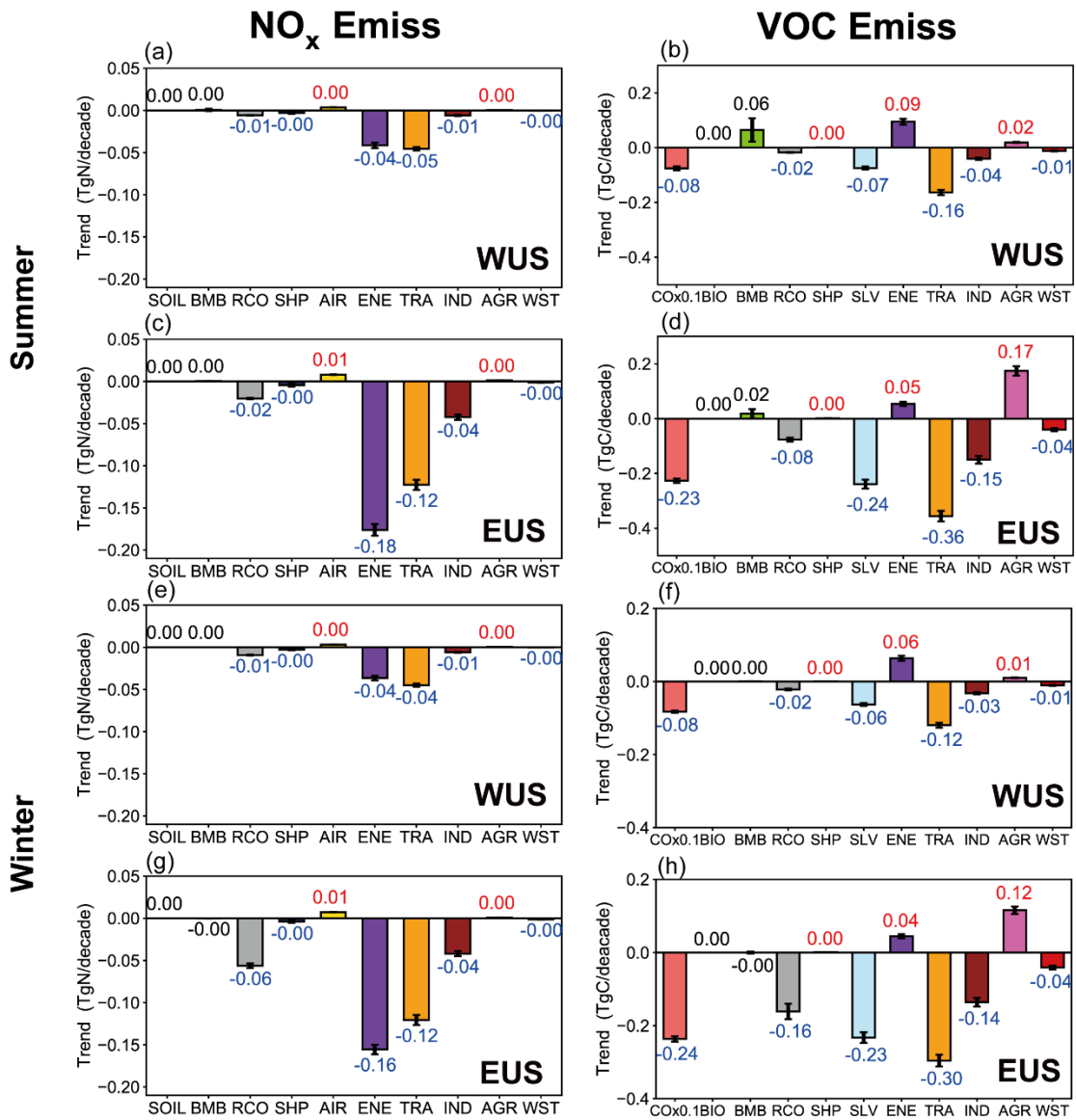
1018  
 1019  
 1020  
 1021  
 1022  
 1023  
 1024  
 1025  
 1026

**Figure 2.** The simulated (contours) and observed (scatters) seasonal mean near-surface O<sub>3</sub> mixing ratios over the United States in JJA (left) and DJF (right) and in 1995 (top) and 2019 (bottom). The correlation coefficient and normalized mean bias (NMB,  $\frac{\sum (\text{Model} - \text{Observation})}{\sum \text{Observation}} \times 100\%$ ) are shown on top right of each panel.



1027  
 1028  
 1029  
 1030  
 1031  
 1032  
 1033  
 1034  
 1035  
 1036  
 1037  
 1038

**Figure 3.** Linear trends (ppb/decade) of simulated (contours) and observed (color-filled markers) (a) annual, (b) JJA and (c) DJF mean near-surface O<sub>3</sub> concentrations during 1995–2019. Areas without hatches indicate statistical significance with 95% confidence. The boxes in (a) mark the western U.S. (WUS, 100–125°W, 30–45°N) and eastern U.S. (EUS, 70–100°W, 30–45°N), respectively. The observed annual O<sub>3</sub> trends in (a) are derived from IPCC AR6, based on Cooper et al. (2020) and Gaudel et al. (2020) over 1995–2017. The observed seasonal O<sub>3</sub> trends in (b) and (c) are calculated based on the U.S. EPA O<sub>3</sub> measurements over 1995–2019.



1040

1041

1042

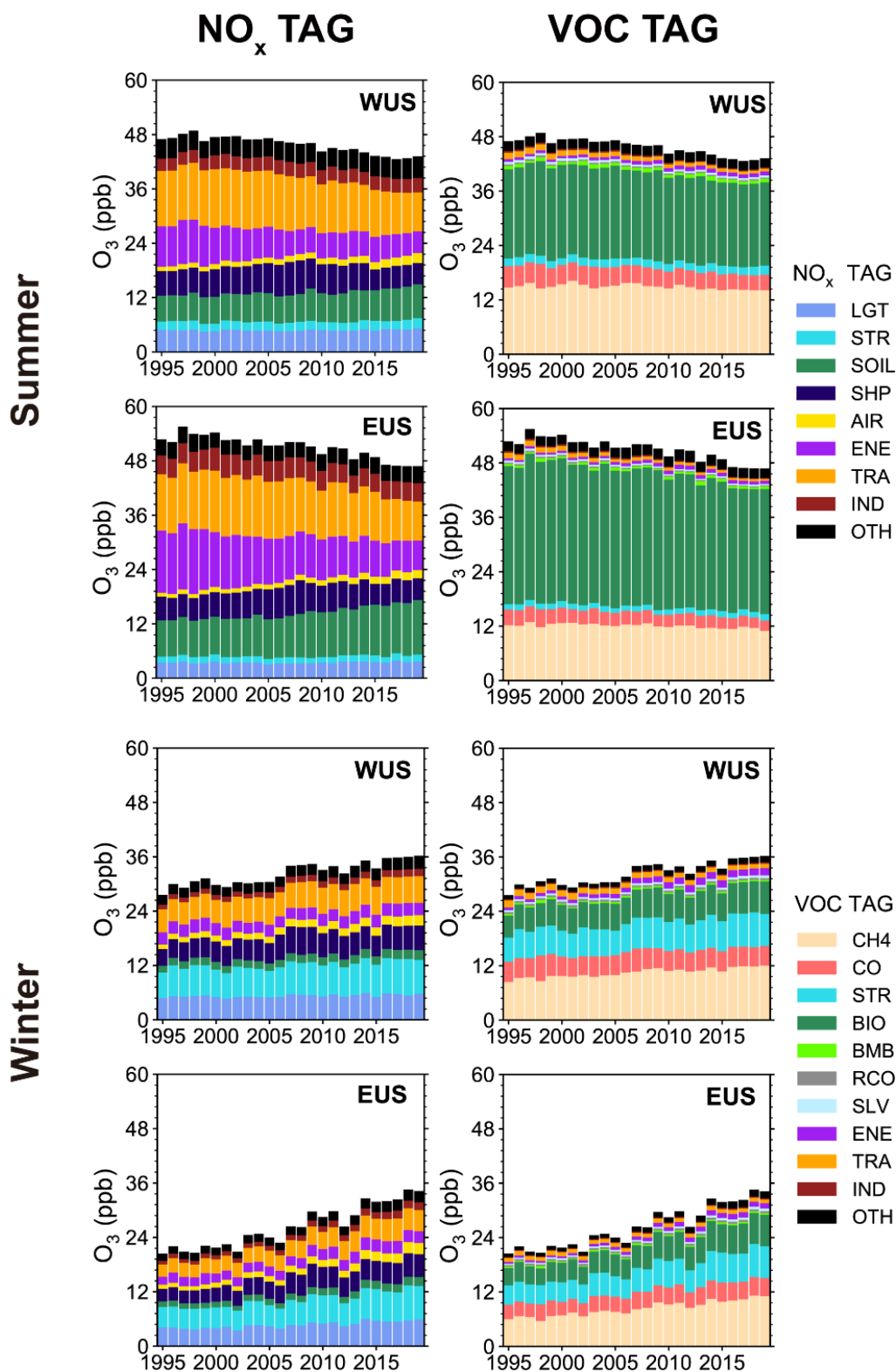
1043

1044

1045

**Figure 34.** Linear trends of NO<sub>x</sub> and reactive carbon emissions from various sectors in summer and winter over WUS and EUS. The increasing and decreasing trends marked with red and blue values, respectively, indicate statistical significance with 95% confidence.





1046

1047

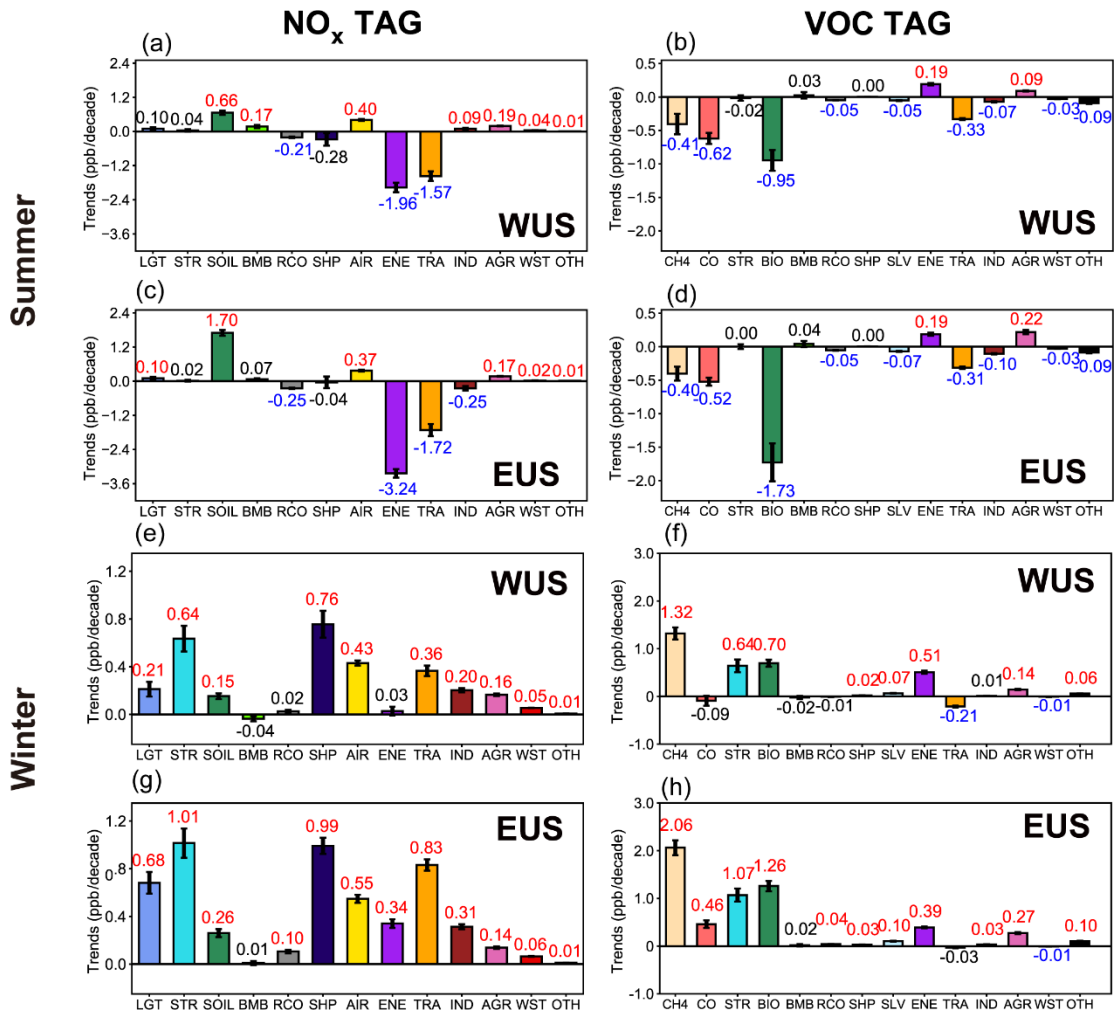
1048

1049

1050

1051

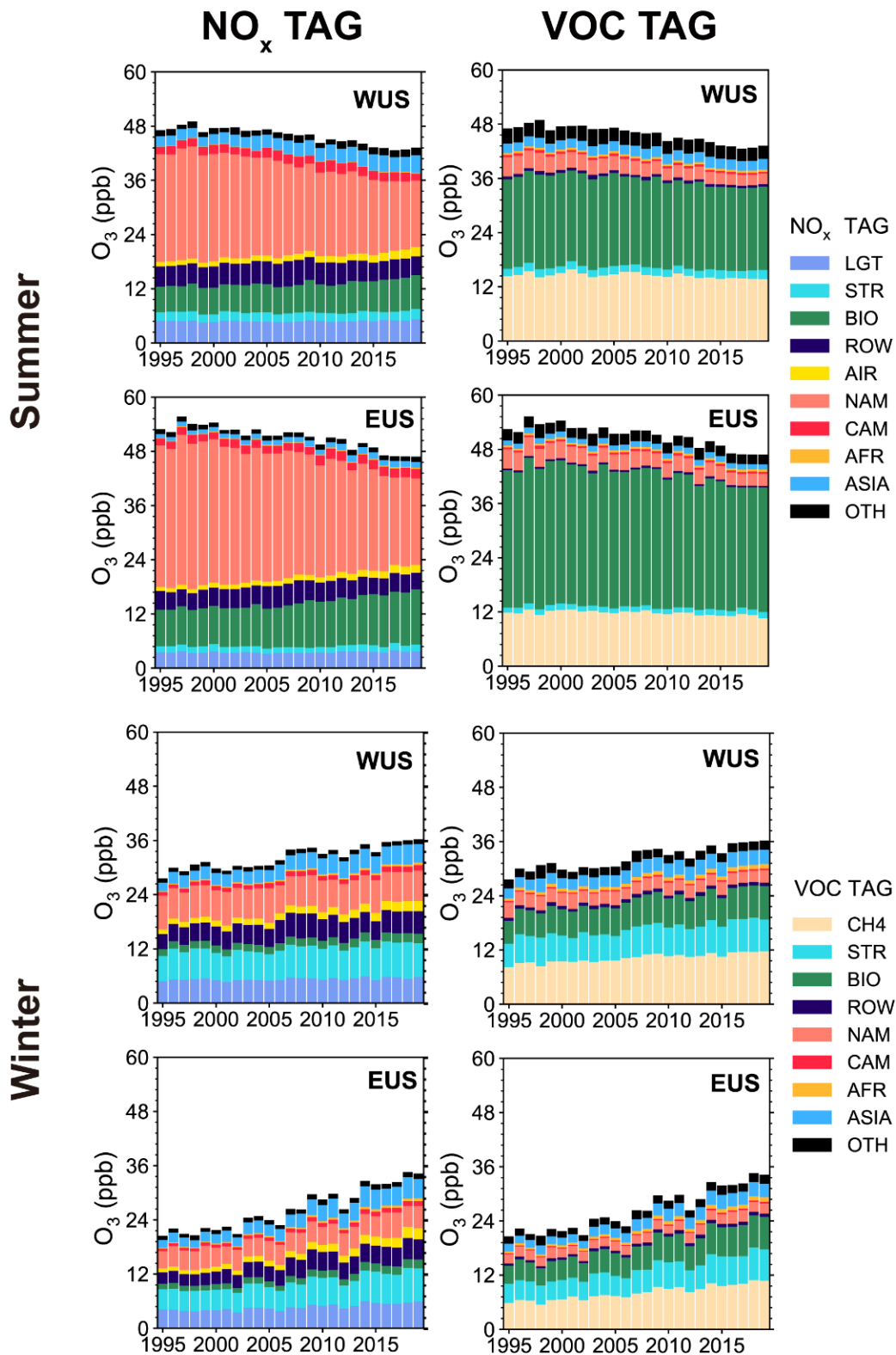
**Figure 45.** Time series of near-surface  $O_3$  concentrations mixing ratios (ppb) averaged over WUS and EUS contributed by  $NO_x$  and reactive carbon emissions from different sectors in summer and winter during 1995–2019. Sources with small contributions are combined and shown as OTH.



1052

1053

1054 **Figure 56.** Linear trends (ppb/decade) of near-surface O<sub>3</sub> concentrations mixing  
 1055 ratios in summer and winter over WUS and EUS contributed by the NO<sub>x</sub> (left)  
 1056 and reactive carbon (right) emissions from various sectors (color bars). The  
 1057 increasing and decreasing trends marked with red and blue color numbers,  
 1058 respectively, indicate statistical significance with 95% confidence. Other  
 1059 sources having small contributions are combined and shown as OTH.



1060

1061

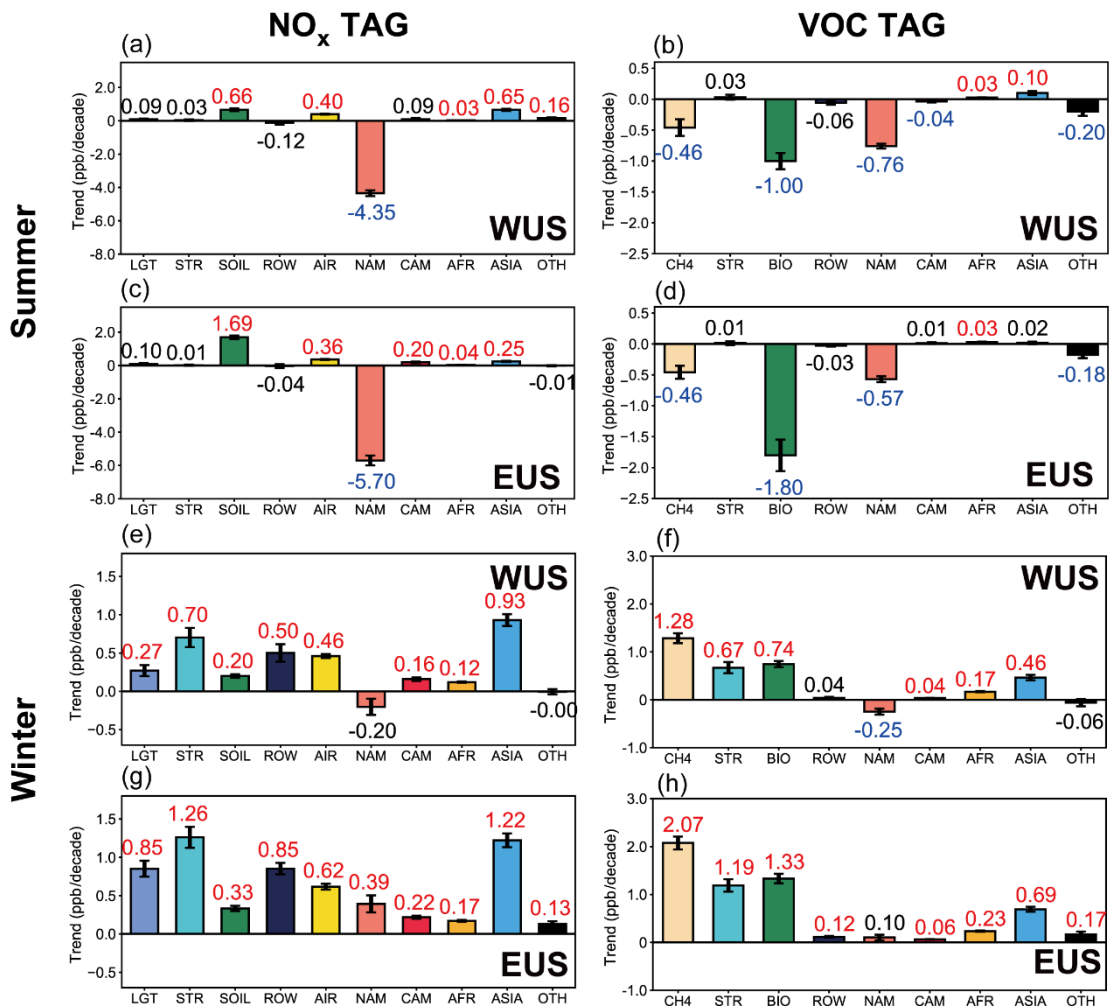
1062

1063

1064

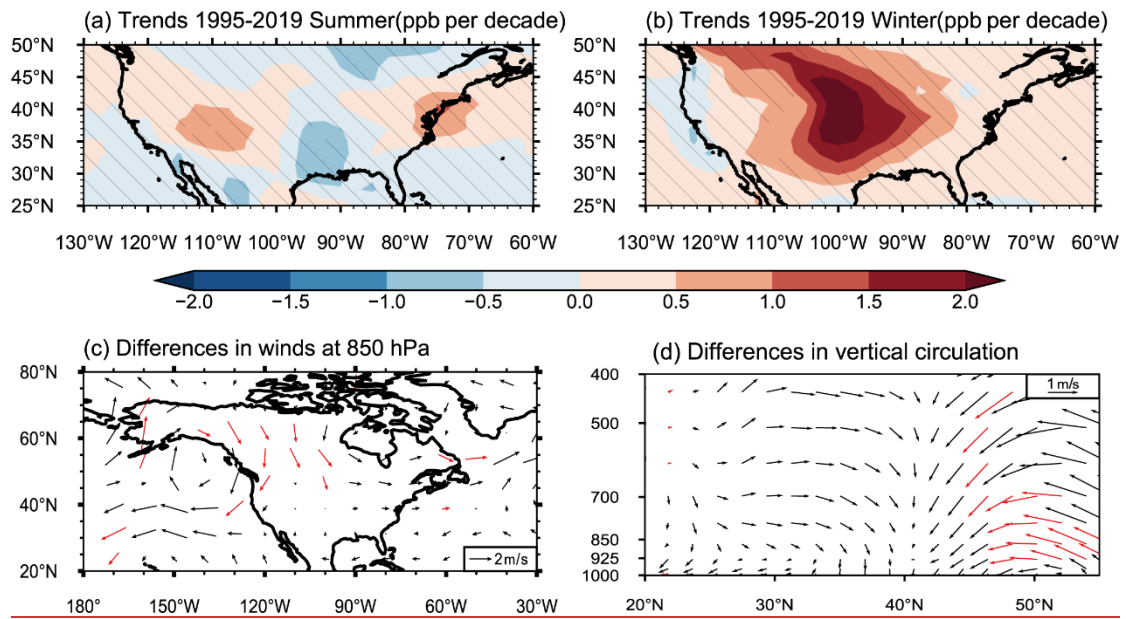
1065

**Figure 67.** Time series of near-surface O<sub>3</sub> concentrations/mixing ratios (ppb) averaged over WUS and EUS contributed by NO<sub>x</sub> and reactive carbon emissions from different source regions in summer and winter during 1995–2019. Sources with small contributions are combined and shown as OTH.



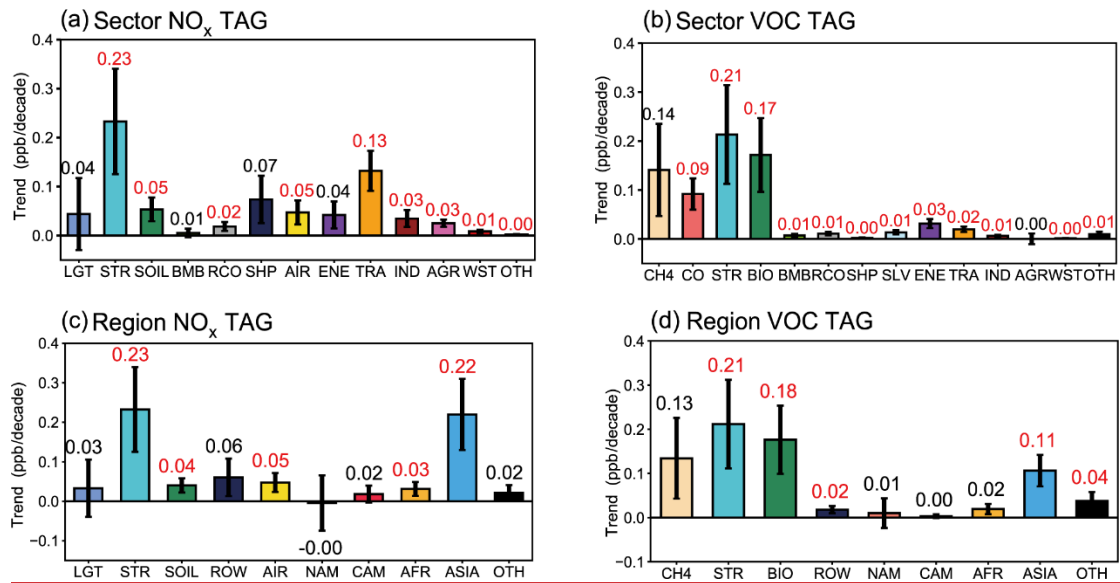
1066  
 1067  
 1068  
 1069  
 1070  
 1071  
 1072  
 1073  
 1074  
 1075  
 1076

**Figure 78.** Linear trends (ppb/decade) of near-surface O<sub>3</sub> concentrations mixing ratios in summer and winter over WUS and EUS contributed by the NO<sub>x</sub> (left) and reactive carbon (right) emissions from various source regions (color bars). The increasing and decreasing trends marked with red and blue color numbers, respectively, indicate statistical significance with 95% confidence. Contributions from source regions EAS, SAS and SEA are combined to ASIA. Other sources having small contributions are combined and shown as OTH.



1077  
 1078  
 1079  
 1080  
 1081  
 1082  
 1083  
 1084  
 1085  
 1086

**Figure 89.** Linear trends (ppb/decade) of simulated (a) JJA and (b) DJF mean near-surface O<sub>3</sub> concentrations during 1995–2019. Differences between the first (1995–1999) and last (2015–2019) five years during 1995–2019 (last–first) in DJF mean (c) 850 hPa horizontal winds and (d) meridional winds and vertical velocity averaged over 90–105°W. Areas without hatches in (a) and (b) and red arrows in (c) and (d) indicate statistical significance with 95% confidence. All results are from the MET experiments.



1087

1088

1089 **Figure 10.** Linear trends (ppb/decade) of near-surface O<sub>3</sub>  
 1090 concentrationsmixing ratios in winter over the U.S, contributed by the NO<sub>x</sub> (e,  
 1091 g,a,c) and reactive carbon (f,h,b,d) emissions from various source sectors (e,  
 1092 fa,b) and regions (g,h,c,d). The increasing and decreasing trends marked with  
 1093 red and blue color numbers, respectively, indicate statistical significance with  
 1094 95% confidence. Contributions from source regions EAS, SAS and SEA are  
 1095 combined to ASIA. Some sources having small contributions are combined  
 1096 and shown as OTH.  
 1097